Stable Paramagnetic Half-Sandwich Mo(V) and W(V) Polyhydride Complexes. Structural, Spectroscopic, Electrochemical, Theoretical, and Decomposition Mechanism Studies of $[Cp^*MH_3(dppe)]^+$ (M = Mo, W)

Brett Pleune,[1a] Dolores Morales,[1b] Rita Meunier-Prest,[1b] Philippe Richard,[1b] Edmond Collange,[1b] James C. Fettinger,[1a] and Rinaldo Poli*,[1b]

Contribution from the Laboratoire de Synthèse et d'Electrosynthèse Organométalliques, Faculté des Sciences "Gabriel", Université de Bourgogne, 6 Boulevard Gabriel, 21000 Dijon, France, and Department of Chemistry and Biochemistry, University of Maryland, College Park, Maryland 20742

Received October 2, 1998

Abstract: Compounds $Cp^*MH_3(dppe)$ (M = Mo, **1**; W, **2**) are oxidized chemically and electrochemically to the corresponding 17-electron cations $\mathbf{1}^+$ and $\mathbf{2}^+$. Analogous oxidations of **1**-d_3 and **2**-d_3 provide $\mathbf{1}^+$-d_3 and $\mathbf{2}^+$-d_3, respectively. Complex $\mathbf{2}^+$ is stable in CH_2Cl_2, THF, and MeCN at room temperature. A single-crystal X-ray analysis of the PF_6^- salt of $\mathbf{2}^+$ shows a geometry for the cation which is intermediate between octahedral and trigonal prismatic, which is reproduced by geometry optimization of the $[CpWH_3(PH_2CH_2CH_2PH_2)]^+$ model at the B3LYP/LANL2DZ level. Identical calculations on the neutral analogue also reproduce the previously reported trigonal prismatic structure for **1**. A blue shift in the M−H stretching vibrations upon oxidation for both Mo and W compounds indicates that a M−H bond strengthening accompanies the oxidation process. The DFT calculations (M−H bond lengths, BDE, and stretching frequencies) are in good agreement with the experimental results. Complex $\mathbf{1}^+$ decomposes in solution at room temperature by one or more of three different mechanisms depending on conditions: H_2 reductive elimination, solvent-assisted disproportionation, or deprotonation. In THF or CH_2Cl_2, a reductive elimination of H_2 affords the stable paramagnetic monohydride $Cp^*MoH(dppe)PF_6$ (**3**), which adds a molecule of solvent in CH_2Cl_2, THF, and MeCN. EPR studies show that the CH_2Cl_2 molecule coordinates in a bidentate mode to afford a 19-electron configuration. A solvent dependence of the decomposition rate [$k(CH_2Cl_2) \approx 7.8k$(THF) at 0 °C] and an inverse isotope effect [$k_H/k_D = 0.50(3)$ in CH_2Cl_2 at 0 °C] indicate the nature of $\mathbf{1}^+$ as a classical trihydride and suggest a decomposition mechanism which involves equilibrium conversion to a nonclassical intermediate followed by a rate-determining associative exchange of H_2 with a solvent molecule. In MeCN at 20 °C, a solvent-assisted disproportionation (rate = $k_{disp}[\mathbf{1}^+]^2$, $k_{disp} = 3.98(9) \times 10^3\ s^{-1}\ M^{-1}$) and a deprotonation by residual unoxidized **1** (rate = $k_{deprot}[\mathbf{1}^+][\mathbf{1}]$, $k_{deprot} = 2.8(2) \times 10^2\ s^{-1}\ M^{-1}$) take place competitively, as shown by detailed cyclic voltammetric and thin-layer cyclic voltammetric studies. The stoichiometric chemical oxidation of **1** in MeCN leads to a mixture of $[Cp^*MoH_2(dppe)(MeCN)]^+$ and $[Cp^*MoH(dppe)(MeCN)_2]^{2+}$ by the disproportionation mechanism.

Introduction

Sparked by the potentials of industrial catalysis, reversible hydrogen storage, and the development of biomimetic hydrogen activating systems, the interest in transition metal hydride complexes has led to tremendous advances in the past 15−20 years, ranging from the existence and properties of coordinated H_2 ligands (so-called nonclassical hydride complexes)[2−6] to the existence of stable paramagnetic transition metal mono- and polyhydride complexes,[7−11] and from the mechanism of fluxional rearrangements[12−14] to $M-H^{\delta-}\cdots H^{\delta+}$ hydrogen bonding.[14−19] The simplicity of the ligand under scrutiny (the hydrogen atom) has made the bond between transition metals and H a favorite subject for a variety of investigations including

* To whom correspondence should be addressed. Tel: +33-03.80.39.68.81. Fax: +33-03.80.39.60.98. E-mail: Rinaldo.Poli@u-bourgogne.fr.

(1) (a) University of Maryland. (b) Université de Bourgogne.
(2) Kubas, G. J.; Ryan, R. R.; Swanson, B. I.; Vergamini, P. J.; Wassermann, H. J. *J. Am. Chem. Soc.* **1984**, *106*, 451−452.
(3) Kubas, G. J. *Acc. Chem. Res.* **1988**, *21*, 120−128.
(4) Crabtree, R. H. *Acc. Chem. Res.* **1990**, *23*, 95−101.
(5) Jessop, P. G.; Morris, R. H. *Coord. Chem. Rev.* **1992**, *121*, 155−191.
(6) Heinekey, D. M.; Oldham, W. J. *Chem. Rev.* **1993**, *93*, 913−944.
(7) Luetkens, M. L., Jr.; Elcesser, W. L.; Huffman, J. C.; Sattelberger, A. P. *Inorg. Chem.* **1984**, *23*, 1718−1726.
(8) Sharp, P. R.; Frank, K. G. *Inorg. Chem.* **1985**, *24*, 1808−1813.
(9) Hamon, P.; Toupet, L.; Hamon, J.-R.; Lapinte, C. *Organometallics* **1992**, *11*, 1429−1431.
(10) Rømming, C.; Smith, K.-T.; Tilset, M. *Inorg. Chim. Acta* **1997**, *259*, 281−290.
(11) Menglet, D.; Bond, A. M.; Coutinho, K.; Dickson, R. S.; Lazarev, G. G.; Olsen, S. A.; Pilbrow, J. R. *J. Am. Chem. Soc.* **1998**, *120*, 2086−2089.
(12) Lee, J. C., Jr.; Yao, W.; Crabtree, R. H.; Rüegger, H. *Inorg. Chem.* **1996**, *35*, 695−699.
(13) Gusev, D. G.; Berke, H. *Chem. Ber.* **1996**, *129*, 1143−1155 and references therein.
(14) Bosque, R.; Maseras, F.; Eisenstein, O.; Patel, B. P.; Yao, W.; Crabtree, R. H. *Inorg. Chem.* **1997**, *36*, 5505−5511.
(15) Lough, A. J.; Park, S.; Ramachandran, R.; Morris, R. H. *J. Am. Chem. Soc.* **1994**, *116*, 8356−8357.
(16) Crabtree, R. H.; Siegbahn, P. E. M.; Eisenstein, O.; Rheingold, A. L.; Koetzle, T. F. *Acc. Chem. Res.* **1996**, *29*, 348−354 and references therein.

10.1021/ja9834881 CCC: $18.00
Published on Web 02/26/1999

structural (X-ray and neutron diffraction and T_1 NMR),[4,20−32] theoretical,[33−39] and reactivity studies including protonation[40−54] and oxidation.[10,55−76] Yet, investigations in this field continue to produce surprises. In this contribution, we present a comprehensive study of the oxidation of $Cp^*MH_3(dppe)$ (M = Mo, W) systems, which provides relevant new information on the structure, stability, M−H bond strength, and decomposition mechanism of paramagnetic polyhydride systems. Steric effects are shown to protect a paramagnetic polyhydride system, in the absence of electronically stabilizing π-donating ligands, against the deprotonation and the disproportionation decomposition pathways; the M−H interaction is unambiguously shown to strengthen upon one-electron oxidation; and the H_2 reductive elimination process has been kinetically assessed for the first time for a paramagnetic polyhydride system. A preliminary report on some aspects of this work has recently appeared.[77]

Experimental Section

General Procedures. Unless otherwise stated, all manipulations were carried out under an inert atmosphere of dinitrogen or argon by the use of Schlenk line or glovebox techniques. Methanol was degassed by three freeze−pump−thaw cycles prior to use. Other solvents were dried by conventional methods (Et_2O from Na/K/benzophenone, toluene and heptane from Na, MeCN from CaH_2, and CH_2Cl_2 from P_4O_{10}) and distilled under dinitrogen prior to use. Deuterated solvents were dried over molecular sieves and degassed by three freeze−pump−thaw cycles prior to use. ^1H and $^{31}P\{^1H\}$ NMR measurements were carried out on Bruker AF200, WP200, or AM400 spectrometers; the peak positions are reported with positive shifts downfield of TMS as calculated from the residual solvent peaks (^1H) or downfield of external 85% H_3PO_4 (^{31}P). For each ^{31}P NMR spectrum, a sealed capillary containing 85% H_3PO_4 was immersed in the same NMR solvent as that used for the measurement, and this was used as the reference. EPR measurements were carried out at the X band microwave frequency on a Bruker ER 200 D spectrometer upgraded to ESP 300, equipped with a cylindrical ER/4103 TM 110 cavity. The spectrometer frequency was calibrated with DPPH ($g = 2.004$). Cyclic voltammograms were obtained at 20 °C in a three-electrode cell with an EG&G 283 potentiostat connected to a personal computer. The working electrode was a 3-mm-diameter carbon disk or a 0.5-mm-diameter platinum disk. Bu_4NPF_6 was used as supporting electrolyte at a concentration of 0.1 M. All potentials are reported vs the Cp_2Fe/Cp_2Fe^+ couple, which has an $E_{1/2}$ of +0.50 V relative to SCE under conditions identical to those of the other experiments. The cyclic voltammograms were fitted by simulations performed with the DIGISIM 2.1 software (BAS Inc.).[78] The solid-state magnetic susceptibility measurements were carried out with a Johnson Matthey magnetic susceptibility balance. The solution conductivity measurements were carried out at 25 °C with a Tacussel type

(17) Patel, B. P.; Kavallieratos, K.; Crabtree, R. H. *J. Organomet. Chem.* **1997**, *528*, 205−207.
(18) Crabtree, R. H. *J. Organomet. Chem.* **1998**, *577*, 111−115.
(19) Chu, H. S.; Lau, C. P.; Wong, K. Y.; Wong, W. T. *Organometallics* **1998**, *17*, 2768−2777.
(20) Hamilton, D. G.; Crabtree, R. H. *J. Am. Chem. Soc.* **1988**, *110*, 4126−4133.
(21) Bautista, M. T.; Earl, K. A.; Maltby, P. A.; Morris, R. H.; Schweitzer, C. T.; Sella, A. *J. Am. Chem. Soc.* **1988**, *110*, 7031−7036.
(22) Bautista, M. T.; Cappellani, E. P.; Drouin, S. D.; Morris, R. H.; Schweitzer, C. T.; Sella, A.; Zubkowski, J. *J. Am. Chem. Soc.* **1991**, *113*, 4876−4887.
(23) Gusev, D. G.; Vymenits, A. B.; Bakhmutov, V. I. *Inorg. Chim. Acta* **1991**, *179*, 195−201.
(24) Desrosiers, P. J.; Cai, L.; Lin, Z.; Richards, R.; Halpern, J. *J. Am. Chem. Soc.* **1991**, *113*, 4173−4184.
(25) Brammer, L.; Howard, J. A. K.; Johnson, O.; Koetzle, T. F.; Spencer, J. L.; Stringer, A. M. *J. Chem. Soc., Chem. Commun.* **1991**, 241−243.
(26) Brammer, L.; Zhao, D.; Bullock, R. M.; McMullan, R. K. *Inorg. Chem.* **1993**, *32*, 4819−4824.
(27) Shin, J. H.; Parkin, G. *Polyhedron* **1994**, *13*, 1489−1493.
(28) Jiménez-Tenorio, M.; Puerta, M. C.; Valerga, P. *Organometallics* **1994**, *13*, 3330−3337.
(29) Klooster, W. T.; Koetzle, T. F.; Jia, G.; Fong, T. P.; Morris, R. H.; Albinati, A. *J. Am. Chem. Soc.* **1994**, *116*, 7677−7681.
(30) Lemke, F. R.; Brammer, L. *Organometallics* **1995**, *14*, 3980−3987.
(31) Luo, X.-L.; Crabtree, R. H. *J. Am. Chem. Soc.* **1990**, *112*, 4813−4821.
(32) Gusev, D. G.; Nietlispach, D.; Eremenko, I. L.; Berke, H. *Inorg. Chem.* **1993**, *32*, 3628−3636.
(33) Hay, J. P. *J. Am. Chem. Soc.* **1987**, *109*, 705−710.
(34) Haynes, G. R.; Martin, R. L.; Hay, P. J. *J. Am. Chem. Soc.* **1992**, *114*, 28−36.
(35) Craw, J. S.; Bacskay, G. B.; Hush, N. S. *J. Am. Chem. Soc.* **1994**, *116*, 5937−5948.
(36) Lin, Z. Y.; Hall, M. B. *Coord. Chem. Rev.* **1994**, *135*, 845−879 and references therein.
(37) Bayse, C. A.; Couty, M.; Hall, M. B. *J. Am. Chem. Soc.* **1996**, *118*, 8916−8919.
(38) Dapprich, S.; Frenking, G. *Organometallics* **1996**, *15*, 4547−4551.
(39) Gelabert, R.; Moreno, M.; Lluch, J. M.; Lledós, A. *J. Am. Chem. Soc.* **1997**, *119*, 9840−9847.
(40) Allison, J. D.; Walton, R. A. *J. Chem. Soc., Chem. Commun.* **1983**, 401−403.
(41) Parkin, G.; Bercaw, J. E. *Polyhedron* **1988**, *7*, 2053−2082.
(42) Jia, G.; Morris, R. H. *J. Am. Chem. Soc.* **1991**, *113*, 875−883.
(43) Jia, G.; Lough, A. J.; Morris, R. H. *Organometallics* **1992**, *11*, 161−171.
(44) Michos, D.; Luo, X.-L.; Faller, J. W.; Crabtree, R. H. *Inorg. Chem.* **1993**, *32*, 1370−1375.
(45) Chin, B.; Lough, A. J.; Morris, R. H.; Schweitzer, C. T.; D'Agostino, C. *Inorg. Chem.* **1994**, *33*, 6278−6288.
(46) Christ, M. L.; Sabo-Etienne, S.; Chaudret, B. *Organometallics* **1994**, *13*, 3800−3804.
(47) Kiss, G.; Nolan, S. P.; Hoff, C. D. *Inorg. Chim. Acta* **1994**, *227*, 285−292.
(48) Feracin, S.; Burgi, T.; Bakhmutov, V. I.; Eremenko, I.; Vorontsov, E. V.; Vimenits, A. B.; Berke, H. *Organometallics* **1994**, *13*, 4194−4202.
(49) Angelici, R. J. *Acc. Chem. Res.* **1995**, *28*, 51−60.
(50) Rothfuss, H.; Gusev, D. G.; Caulton, K. G. *Inorg. Chem.* **1995**, *34*, 2894−2901.
(51) Shubina, E. S.; Krylov, A. N.; Belkova, N. V.; Epstein, L. M.; Borisov, A. P.; Mahaev, V. D. *J. Organomet. Chem.* **1995**, *493*, 275−277.
(52) Bullock, R. M.; Song, J.-S.; Szalda, D. J. *Organometallics* **1996**, *15*, 2504−2516.
(53) Castillo, A.; Esteruelas, M. E.; Oñate, E.; Ruiz, N. *J. Am. Chem. Soc.* **1997**, *119*, 9691−9698.
(54) Luther, T. A.; Heinekey, D. M. *Inorg. Chem.* **1998**, *37*, 127−132.
(55) Sanders, J. R. *J. Chem. Soc., Dalton Trans.* **1973**, 748−749.
(56) Sanders, J. R. *J. Chem. Soc., Dalton Trans.* **1975**, 2340−2342.
(57) Pilloni, G.; Schiavon, G.; Zotti, G.; Zecchin, S. *J. Organomet. Chem.* **1977**, *134*, 305−318.
(58) Klinger, R. J.; Huffman, J. C.; Kochi, J. K. *J. Am. Chem. Soc.* **1980**, *102*, 208−216.
(59) Allison, J. D.; Cameron, C. J.; Wild, R. E.; Walton, R. A. *J. Organomet. Chem.* **1981**, *218*, C62−C66.
(60) Rhodes, L. F.; Zubkowski, J. D.; Folting, K.; Huffman, J. C.; Caulton, K. G. *Inorg. Chem.* **1982**, *21*, 4185−4192.
(61) Bruno, J. W.; Caulton, K. G. *J. Organomet. Chem.* **1986**, *315*, C13−C16.
(62) Lemmen, T. H.; Lundquist, L. F.; Sutherland, B. R.; Westerberg, D. E.; Caulton, K. G. *Inorg. Chem.* **1986**, *25*, 3915−3917.
(63) Detty, M. R.; Jones, W. D. *J. Am. Chem. Soc.* **1987**, *109*, 5666−5673.
(64) Costello, M. T.; Walton, R. A. *Inorg. Chem.* **1988**, *27*, 2563−2564.
(65) Chen, L.; Davies, J. A. *Inorg. Chim. Acta* **1990**, *175*, 41−45.
(66) Roullier, L.; Lucas, D.; Mugnier, Y.; Antiñolo, A.; Fajardo, M.; Otero, A. *J. Organomet. Chem.* **1990**, *396*, C12−C16.
(67) Tilset, M.; Parker, V. D. *J. Am. Chem. Soc.* **1990**, *112*, 2843.
(68) Roullier, L.; Lucas, D.; Mugnier, Y.; Antiñolo, A.; Fajardo, M.; Otero, A. *J. Organomet. Chem.* **1991**, *412*, 353−362.
(69) Ryan, O. B.; Tilset, M. *J. Am. Chem. Soc.* **1991**, *113*, 9554−9561.
(70) Ryan, O. B.; Tilset, M.; Parker, V. D. *Organometallics* **1991**, *10*, 298−304.
(71) Westerberg, D. E.; Rhodes, L. F.; Edwin, J.; Geiger, W. E.; Caulton, K. G. *Inorg. Chem.* **1991**, *30*, 1107−1112.
(72) Tilset, M. *J. Am. Chem. Soc.* **1992**, *114*, 2740−2741.
(73) Amatore, C.; Fraústo da Silva, J. J. R.; Guedes da Silva, M. F. C.; Pombeiro, A. J. L.; Verpeaux, J.-N. *J. Chem. Soc., Chem. Commun.* **1992**, 1289−1291.
(74) Smith, K.-T.; Tilset, M. *J. Organomet. Chem.* **1992**, *431*, 55−64.
(75) Smith, K.-T.; Rømming, C.; Tilset, M. *J. Am. Chem. Soc.* **1993**, *115*, 8681−8689.
(76) Zlota, A. A.; Tilset, M.; Caulton, K. G. *Inorg. Chem.* **1993**, *32*, 3816−3821.
(77) Pleune, B.; Poli, R.; Fettinger, J. C. *J. Am. Chem. Soc.* **1998**, *120*, 3257−3258.

CD6 N conductimeter equipped with an XE 110 cell which had been calibrated with a 0.1 M KCl solution. The elemental analyses were carried out by Desert Analytics (Tucson, AZ), by Atlantic Microlab (Norcross, GA), or by the analytical service of the Laboratoire de Synthèse et d'Electrosynthèse Organométalliques (LSEO) of the Université de Bourgogne. $LiAlD_4$ and CH_3OD (Aldrich) were used as received, without further purification. $[Cp_2Fe]PF_6$,[79] $CDFCl_2$,[80] and $Cp^*MH_3(dppe)$ (M = Mo, **1**; W, **2**)[81] were prepared according to literature procedures.

Synthesis of $Cp^*MoD_3(dppe)$ (1-d_3). This reaction follows the protocol reported previously for the preparation of $Cp^*MoH_3(dppe)$.[81] Cp^*MoCl_4 (555 mg, 1.488 mmol), dppe (592 mg, 1.488 mmol), and $LiAlD_4$ (0.6 g, 14.3 mmol) were slurried in a 70 mL:15 mL toluene/diethyl ether solvent mixture at room temperature. The mixture was stirred for 12 h, and CH_3OD (3 mL) as added dropwise to the stirring mixture at room temperature, causing a vigorous gas evolution. The solvent mixture was removed under reduced pressure, and the residue was extracted with heptane (100 mL). The heptane solution was filtered through Celite and concentrated to ca. 1 mL, precipitating a yellow powder, which was washed with cold (−80 °C) heptane and dried under vacuum. Yield: 480 mg (51%). The NMR properties of **1**-d_3 are identical with those of **1**,[81] except for the undetectable hydride resonances in the ^1H NMR and the P−D coupling in the $^{31}P\{^1H\}$ NMR spectra. ^1H NMR (C_6D_6, δ): 7.8−7.0 (m, Ph, 20H), 2.05−1.75 (m, CH_2, 4H), 1.84 (s, Cp*, 15H). $^{31}P\{^1H\}$ NMR (C_6D_6, δ): 92.1 (1:3:6:7:6:3:1 septet, J_{PD} =12.3 Hz).

Synthesis of $Cp^*WD_3(dppe)$ (2-d_3). This reaction follows the protocol reported previously for the preparation of $Cp^*MoH_3(dppe)$.[81] Cp^*WCl_4 (282 mg, 0.612 mmol), dppe (243 mg, 0.612 mmol), and $LiAlD_4$ (0.3 g, 7.1 mmol) were slurried in a 100 mL:15 mL toluene/diethyl ether solvent mixture at room temperature. The mixture was stirred for 12 h, and CH_3OD (0.5 mL) was added to the stirring mixture, causing gas evolution. The solvent mixture was then removed under reduced pressure, and the residue was extracted into heptane (100 mL). The heptane solution was filtered through Celite and concentrated to ca. 0.5 mL, precipitating an orange powder which was washed with cold (−80 °C) heptane and dried under vacuum. Yield: 91 mg (21%). To the remaining residue was added 75 mL of heptane, and 3 mL of CH_3OD was added dropwise at room temperature. Gas vigorously evolved, and the solution developed a red-orange color. The reaction mixture was stirred for an additional 30 min and then filtered through Celite. The solution was evaporated to ca. 0.5 mL, precipitating a second crop of orange powder (116 mg). Combined yield: 207 mg (47%). The NMR properties of **2**-d_3 are identical to those of **2**,[81] except for the undetectable hydride resonances in the ^1H NMR and the P−D coupling in the $^{31}P\{^1H\}$ NMR spectra. ^1H NMR (C_6D_6, δ): 7.8−7.0 (m, Ph, 20H), 2.25−2.00 (m, CH_2, 4H), 1.96 (s, 15H, Cp*). $^{31}P\{^1H\}$ NMR (C_6D_6, δ): 67.9 (1:3:6:7:6:3:1 septet, J_{PD} = 8.2 Hz).

Chemical Oxidation of 1 in THF at −80 °C. Cp_2FePF_6 (0.025 g, 0.075 mmol) was added to a stirring solution of **1** (0.047 g, 0.074 mmol) in THF (1 mL) at −80 °C. An immediate reaction occurred which quenched the blue color of the Cp_2FePF_6. This solution exhibited a triplet of quartets in the EPR spectrum at −80 °C (g = 1.989, a_P (triplet) = 28.9 G, a_H (quartet) = 11.8 G), attributable to $[Cp^*MoH_3(dppe)][PF_6]$ (**1**$^+$). This spectrum is shown in Figure 1. IR (THF, cm^{-1}): 1896 (w, sh), 1824 (m, broad). The spectrum was recorded immediately after charging the cell with the cold solution. By comparison, a solution of compound 1 showed M−H stretching vibrations at 1775 and 1815 cm^{-1} (see Figure 2).

Chemical Oxidation of 1 in THF at Room Temperature. Cp_2FePF_6 (0.029 g, 0.087 mmol) was added to a stirring solution of **1** (0.055 g, 0.087 mmol) in THF (1 mL) at room temperature. An immediate reaction occurred which quenched the blue color of the Cp_2FePF_6. An aliquot of this solution was immediately transferred into an EPR tube and frozen at the liquid nitrogen temperature until prior to the insertion into the EPR probe. The resulting spectrum showed **1**$^+$ as the only paramagnetic product. The solution gradually developed a red-

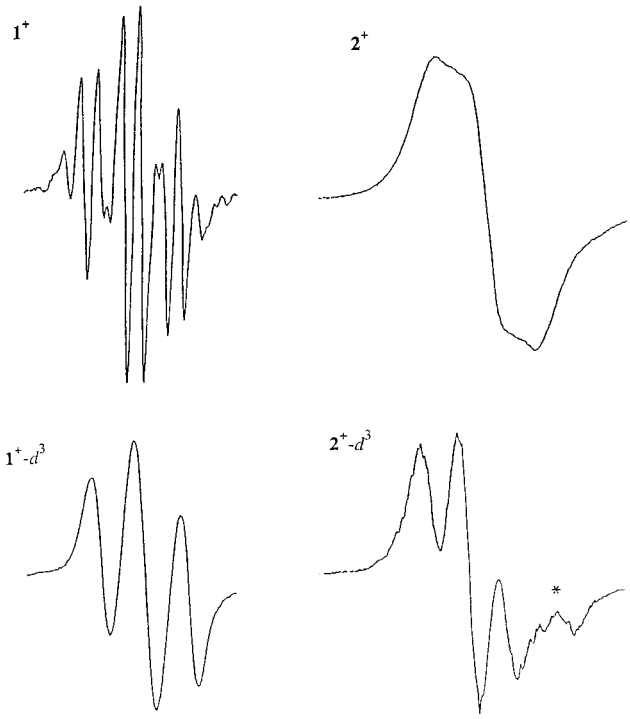

Figure 1. Room-temperature EPR spectra of compounds $[Cp^*MX_3(dppe)]^+$ (M = Mo, X = H, **1**$^+$; D, **1**$^+$-d_3. M = W, X = H, **2**$^+$; D, **2**$^+$-d_3) in THF. The asterisk in the spectrum of **2**$^+$-d_3 indicates an unknown impurity.

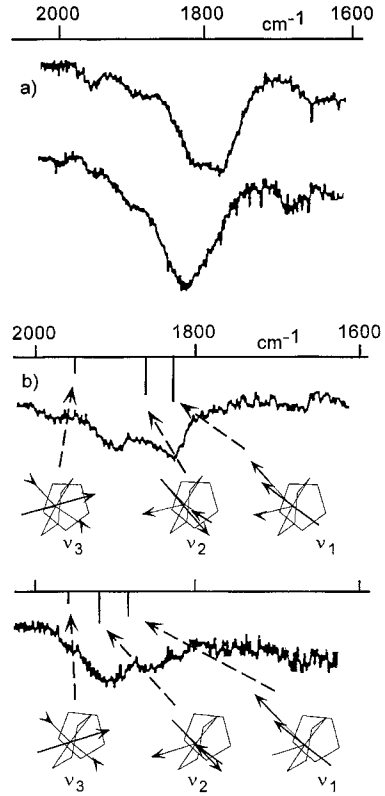

Figure 2. Room-temperature IR spectra of (a) **1** (top) and **1**$^+$ (bottom) in THF and (b) **2** (top) and **2**$^+$ (bottom) in THF. The normal modes and relative intensities corresponding to the frequencies ν_1, ν_2, and ν_3 in part b are obtained from DFT calculations on geometry-optimized $[CpWH_3(H_2PCH_2CH_2PH_2)]^{n+}$ (n = 0, 1; see text).

(78) Rudolph, M.; Reddy, D. P.; Feldberg, S. W. *Anal. Chem.* **1994**, *66*, 589A−600A.

(79) Yang, E. S.; Chan, M.; Wahl, A. C. *J. Phys. Chem.* **1975**, *79*, 2049−2051.

(80) Siegel, S. S.; Anet, F. A. *J. Org. Chem.* **1988**, *53*, 2629−2630.

(81) Pleune, B.; Poli, R.; Fettinger, J. C. *Organometallics* **1997**, *16*, 1581−1594.

orange color, which was accompanied by gas evolution. EPR monitoring showed decomposition to afford a new EPR signal consisting of a doublet of triplets ($g = 1.950$, $a_P = 16.5$ G, $a_H = 24.0$ G), which is attributed to $[Cp^*MoH(dppe)(THF)]^+$ (vide infra).

Chemical Oxidation of 1 in CH_2Cl_2 at Room Temperature. Cp_2FePF_6 (0.024 g, 0.071 mmol) was added to a stirring solution of **1** (0.045 g, 0.071 mmol) in CH_2Cl_2 (1 mL) at room temperature. An immediate reaction occurred which quenched the blue color of the Cp_2FePF_6, followed by gas evolution. The solution gradually developed a red-orange color. EPR monitoring as described in the previous section showed initially $\mathbf{1}^+$ as the only paramagnetic product. This was followed by rapid decomposition, with gas evolution, to afford a new EPR signal consisting of a doublet of triplets ($g = 1.950$, $a_P = 16.5$ G, $a_H = 24.0$ G). In a separate experiment, 0.5 mL of CD_2Cl_2 was trasferred via cannula into an NMR tube containing **1** (0.040 g, 0.063 mmol) and Cp_2FePF_6 (0.021 g, 0.063 mmol) at −80 °C, which was then further cooled to −196 °C, and the tube was flame-sealed under vacuum. The tube was subsequently warmed to room temperature, resulting in gas evolution over a 30−45-min period. ^{1}H NMR spectroscopy exhibited a resonance (δ 4.61) due to the formation of H_2 gas as a product of this reaction. A control experiment in which H_2 gas was bubbled directly into CD_2Cl_2 exhibited a resonance at δ 4.60 in the ^{1}H NMR spectrum.

Chemical Oxidation of 1-d_3 in THF at −80 °C. Cp_2FePF_6 (0.016 g, 0.049 mmol) was added to a stirring solution of **1**-d_3 (0.031 g, 0.049 mmol) in THF (1 mL) at −80 °C. An immediate reaction occurred which quenched the blue color of the Cp_2FePF_6. An aliquot of this solution was transferred into an EPR tube which was maintained at −80 °C. The EPR spectrum at −80 °C consisted of a broad triplet ($g = 1.991$, $a_P = 28.9$ G), attributable to $[Cp^*MoD_3(dppe)][PF_6]$ ($\mathbf{1}^+$-d_3) (Figure 1). IR (THF, cm^{-1}): 1318 (m, broad). The spectrum was recorded immediately after the cell was charged with the cold solution. By comparison, a solution of compound **1**-d_3 showed a M−H stretching vibration centered at 1307 cm^{-1}. Upon the solution warming to room temperature, the EPR signal due to $\mathbf{1}^+$-d_3 disappeared rapidly and was replaced by a binomial triplet of 1:1:1 triplets ($g = 1.954$, $a_P = 18.4$ G, $a_D = 4.0$ G), which is assigned to $[Cp^*MoD(dppe)(THF)]^+$, followed by further decomposition (vide infra).

Synthesis of {Cp*MoH(dppe)PF_6} (3). Cp_2FePF_6 (0.135 g, 0.407 mmol) was added to a stirring solution of **1** (0.257 g, 0.407 mmol) dissolved in 5 mL of THF at −80 °C. An immediate reaction occurred which quenched the blue color of the Cp_2FePF_6. The solution was allowed to stir for 45 min at −80 °C. The Schlenk flash was then removed from the acetone−dry ice bath, and the solution was allowed to warm to room temperature with stirring for an additional 30 min. The solution gradually evolved gas and developed a red-orange color. After filtration, the solution was concentrated to ca. 2 mL. Heptane (20 mL) was added, precipitating a light purple solid, which was filtered, washed with heptane (3 × 15 mL), and dried in vacuo. Yield: 221 mg (64%). Anal. Calcd for $C_{36}H_{40}F_6MoP_3$: C, 55.8; H, 5.2. Found: C, 55.1; H, 5.3. EPR spectrum (THF, room temperature): dt ($g = 1.950$, $a_P = 16.5$ G, $a_H = 24.0$ G). EPR spectrum (CH_2Cl_2, room temperature): dt ($g = 1.950$, $a_P = 16.5$ G, $a_H = 24.0$ G). EPR spectrum (CH_2Cl_2, 0 °C): dt of 1:2:3:4:3:2:1 septets ($g = 1.950$, $a_P = 16.5$ G, $a_H = 24.0$ G, $a_{Cl} = 1.0$ G). Next, 135 mg (0.174 mmol) of this solid was dissolved in 0.5 mL of MeCN at room temperature, forming a red solution. The EPR spectrum of this solution was identical, within experimental error, to the spectra of the THF and CH_2Cl_2 solutions. Et_2O (15 mL) was added to the stirring solution, precipitating a red-brown solid, which was washed with Et_2O (2 × 5 mL). Yield: 49 mg (36%). The solids crystallized from THF and from MeCN have identical IR spectra in Nujol mull. $\mu_{eff} = 1.50$ μ_B. No diamagnetic impurities were detected in the ^{1}H NMR spectrum (CD_3CN). Molar conductivity (Λ, S cm^2 mol^{-1}, CH_2Cl_2): 15.5 (7.1×10^{-3} M); 29.1 (7.1×10^{-4} M). $\Lambda_\infty = 35.4$ S cm^2 mol^{-1}.

Chemical Oxidation of 1 in MeCN at Room Temperature. Cp_2FePF_6 (0.027 g, 0.081 mmol) was added to a stirring slurry of **1** (0.051 g, 0.081 mmol) in MeCN (1 mL) at room temperature. An immediate reaction occurred which dissolved the insoluble yellow precipitate; the solution turned orange. Gas evolution was noted during this period, which ceased almost immediately (a few seconds). An EPR spectrum of this solution did not exhibit any detectable resonances. After evaporation of the mixture to dryness, an NMR investigation (both ^{1}H NMR and ^{31}P NMR) of the residue in CD_3CN revealed the resonances of the previously described[81] complexes $[Cp^*MoH_2(MeCN)(dppe)]^+$ and $[Cp^*MoH(MeCN)_2(dppe)]^{2+}$ in a ca. 17:83 ratio. No other species were detected in the NMR spectra.

Chemical Oxidation of Compound 2 at Room Temperature. Synthesis of $[Cp^*WH_3(dppe)][PF_6]$ ($\mathbf{2}^+PF_6^-$). To a yellow-orange solution of **2** (115 mg, 0.160 mmol) in 4 mL of CH_2Cl_2 was added Cp_2FePF_6 (53 mg, 0.160 mmol) at room temperature. The solution immediately turned red-orange. The solution was filtered and concentrated under reduced pressure to ca. 0.5 mL. Orange single crystals of $\mathbf{2}^+PF_6^-$ were obtained by diffusion of a layer of diethyl ether into this solution. Yield: 97 mg (70%). A suitable single crystal obtained in this manner was used for the X-ray analysis. EPR spectrum (CH_2Cl_2): triplet (br, $g = 2.017$), see Figure 1. IR (THF, cm^{-1}): 1897 (m, broad), 1830 (w, broad), see Figure 2. By comparison, a solution of compound **2** showed M−H stretching vibrations at 1815 and 1885 cm^{-1} (Figure 2). No diamagnetic impurities were detected in the ^{1}H NMR spectrum (CD_3CN). The oxidation of 2 can also be conducted using THF, MeCN, and acetone as solvents, with identical spectroscopic results.

Chemical Oxidation of Compound 2-d_3 at Room Temperature. To a yellow-orange solution of **2**-d_3 (0.030 g, 0.042 mmol) in 1 mL of CH_2Cl_2 was added Cp_2FePF_6 (0.014 g, 0.042 mmol) at room temperature. The solution immediately turned red-orange. An EPR spectrum of this solution exhibited a broad triplet resonance with distinguishable phosphorus coupling ($g = 2.022$, $a_P = 27.6$ G), see Figure 1, attributable to $[Cp^*WD_3(dppe)][PF_6]$ ($\mathbf{2}^+$-d_3). W−D bands could not be located in the IR spectra for compounds **2**-d_3 and $\mathbf{2}^+$-d_3 (no significant changes were observed upon oxidation).

X-ray Crystallography. Compound $\mathbf{2}^+PF_6^-$. All operations were routine. Crystal parameters and data collection and refinement details are summarized in Table 1. Data were corrected for Lorentz and polarization factors and by absorption (ψ-scan method); a decay correction was not necessary. All H atoms except the three hydride ligands were placed in calculated positions and refined with the riding model. The three hydride ligands were located from the highest peaks near the W atom with W−H distances ranging from 1.4 to 1.7 Å. They were initially refined freely but found to possess varying bond lengths with the W atom, and therefore their refinement was assisted by restraining the W−H distance to be near 1.70 Å (ADFIX with esd of 0.03 Å). Thermal parameters were allowed to refine freely. Selected bond distances and angles for complex $\mathbf{2}^+$ are reported in Table 2.

Compound $[Cp^*WH_4(dppe)]^+PF_6^-$ ($[\mathbf{2}\text{-H}]^+PF_6^-$). Colorless single crystals of this compound were obtained by slow diffusion of a diethyl ether layer into a saturated dichloromethane solution. Crystal parameters and data collection and refinement details are summarized in Table 1. Data were corrected for Lorentz and polarization factors and by absorption (ψ-scan method); no decay correction was necessary. The structure solution and refinement were routine. Handling of the H atoms attached to carbon followed the protocol described above for compound $\mathbf{2}^+PF_6^-$. Four hydride ligands were located at reasonable positions and W−H distances, but an attempted refinement gave wide variations in U's and W−H distances. Attempts at restrained hydride refinement with $d(W-H_{initial}) = 1.75$ Å in SHELXL93 proved futile. The final structure was refined to convergence without the presence of the hydride atoms. Selected bond distances and angles for complex $[\mathbf{2}\text{-H}]^+$ are reported in Table 2.

Computational Details. All the calculations were performed using GAUSSIAN 94[82] on an Origin200 SGI workstation. The LanL2DZ set (basis I) was employed to perform complete geometry optimization with a density functional theory (DFT) approach. The three-parameter

(82) Frisch, M. J.; Trucks, G. W.; Schlegel, H. B.; Gill, P. M. W.; Johnson, B. G.; Robb, M. A.; Cheeseman, J. R.; Keith, T. A.; Petersson, G. A.; Montgomery, J. A.; Raghavachari, K.; Al-Laham, M. A.; Zakrzewski, V. G.; Ortiz, J. V.; Foresman, J. B.; Cioslowski, J.; Stefanov, B. B.; Nanayakkara, A.; Challacombe, M.; Peng, C. Y.; Ayala, P. Y.; Chen, W.; Wong, M. W.; Andres, J. L.; Replogle, E. S.; Gomperts, R.; Martin, R. L.; Fox, D. J.; Binkley, J. S.; Defrees, D. J.; Baker, J.; Stewart, J. P.; Head-Gordon, M.; Gonzales, C.; Pople, J. A. *Gaussian 94 (Revision E.1)*; Gaussian Inc.: Pittsburgh, PA, 1995.

Table 1. Crystal Data and Structure Refinement for $2^+PF_6^-$ and $[2\text{-H}]^+PF_6^-$

	$2^+PF_6^-$	$[2\text{-H}]^+PF_6^-$
empirical formula	$C_{36}H_{42}F_6P_3W$	$C_{36}H_{43}F_6P_3W$
formula weight	865.46	866.46
temperature	153(2) K	153(2) K
wavelength	0.710 73 Å	0.710 73 Å
crystal system, space group	monoclinic, *P*2(1)/*n*	monoclinic, *P*2(1)/*n*
unit cell dimensions	a = 14.3763(8) Å	*a* = 14.4683(15) Å
	b = 16.684(2) Å	*b* = 16.4788(15) Å
	c = 15.0123(12) Å	*c* = 15.0809(15) Å
	β = 100.424(6)°	*β* = 100.140(8)°
volume, *Z*	3541.4(5) Å^3, 4	3539.4(6) Å^3, 4
density (calcd)	1.623 Mg m^{-3}	1.626 Mg m^{-3}
absorption coeff	3.454 mm^{-1}	3.456 mm^{-1}
F(000)	1724	1728
θ range for data colln	1.80−24.99°	1.80−22.50°
reflns collected	19 459	9640
independent reflns	6226 [*R*(int) = 0.0729]	4617 [*R*(int) = 0.0826]
max. and min. transmission	0.4216 and 0.3384	0.3590 and 0.2640
data/restraints/paramrs	6226/4/432	4617/3/423
goodness-of-fit on F^2	1.076	1.056
final *R* indices [$I > 2\sigma(I)$]	*R*1 = 0.0412	*R*1 = 0.0558
	w*R*2 = 0.0767 [4577 data]	w*R*2 = 0.1101 [3033 data]
R indices (all data)	R1 = 0.0713	R1 = 0.1035
	wR2 = 0.0861	wR2 = 0.1265
largest diff peak and hole	1.351 and −0.945 e Å^{-3}	1.380 and −1.002 e Å^{-3}

Table 2. Bond Lengths (Å) and Angles (deg) for $2^+PF_6^-$ and $[2\text{-H}]^+PF_6^-$, and Comparison with the Previously Reported Values for $[2\text{-H}]^+BF_4^-$ [a]

	$2^+PF_6^-$	$[2\text{-H}]^+PF_6^-$	$[2\text{-H}]^+BF_4^-$ [b]
W1−CNT	1.999(15)	1.996(5)	1.990(9)
W(1)−P(1)	2.474(2)	2.484(3)	2.477(2)
W(1)−P(2)	2.506(2)	2.516(3)	2.508(2)
W(1)−H(1)	1.71(2)		
W(1)−H(2)	1.67(3)		
W(1)−H(3)	1.69(3)		
P(1)−W(1)−P(2)	78.85(5)	78.79(11)	78.72(7)
CNT −W1−P1	162.0(2)	163.6(2)	162.8(2)
CNT −W1−P2	119.1(2)	117.7(2)	118.4(2)
CNT−W1−H1	109(2)		
CNT −W1−H2	103(2)		
CNT −W1−H3	113(2)		

[a] CNT is the centroid of atoms C(1)−C(5). [b] From ref 81.

form of the Becke, Lee, Yang, and Parr functional (B3LYP)[83] was employed. The LanL2DZ basis set includes both Dunning and Hay's D95 sets for H and C[84] and the relativistic electron core potential (ECP) sets of Hay and Wadt for the heavy atoms.[85−87] Electrons outside the core were all those of H and C atoms, the 3s and 3p electrons of the P atoms, and the 5s, 5p, 5d and 6s electrons of the W atom. Single-point calculations on the B3LYP/LANL2DZ-optimized geometries were also carried out with an extended basis set (basis II) in which the hydride ligands are represented in a triple-*ξ* basis set. All calculations were carried out without imposed symmetry.

The mean value of the spin of the first-order electronic wave function, which is not an exact eigenstate of S^2 for unrestricted calculations on open-shell systems, was considered suitable for the unambiguous identification of the spin state. Spin contamination was carefully monitored, and the energies shown in the Results section correspond to unrestricted B3LYP (UB3LYP) calculations. The value of $\langle S^2 \rangle$ for the UB3LYP calculations was 0.7546 for $[CpWH_3(H_2PCH_2CH_2PH_2)]^+$, 0.7545 for $CpWH_2(H_2PCH_2CH_2PH_2)$, and 2.0117 and 2.0126 for cis and trans triplet $[CpWH_2(H_2PCH_2CH_2PH_2)]^+$, respectively, indicating minor spin contamination.

(83) Becke, A. D. *J. Chem. Phys.* **1993**, *98*, 5648−5652.
(84) Dunning, T. H., Jr.; Hay, P. J. In *Modern Theoretical Chemistry*; Schaefer, H. F., III, Ed.; Plenum Press: New York, 1976; pp 1−28.
(85) Hay, P. J.; Wadt, W. R. *J. Chem. Phys.* **1985**, *82*, 270−283.
(86) Wadt, W. R.; Hay, P. J. *J. Chem. Phys.* **1985**, *82*, 284−298.
(87) Hay, P. J.; Wadt, W. R. *J. Chem. Phys.* **1985**, *82*, 299−310.

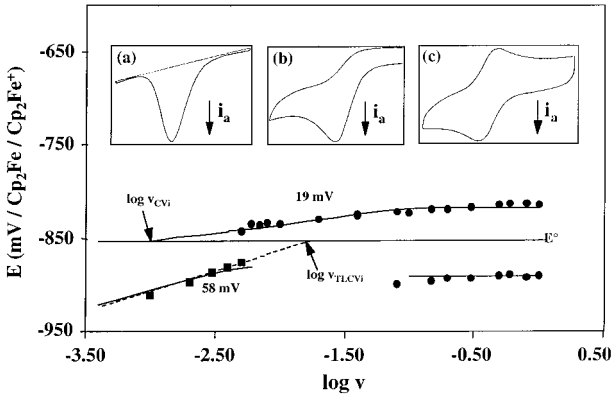

Figure 3. Peak potentials for the oxidation of **1** and reduction of $\mathbf{1}^+$ in MeCN as a function of scan rate (v in V s^{-1}) at [**1**] = 8.9 × 10^{-4} M. Circles refer to CV data, and squares refer to TLCV data. The lines fitting the data are obtained from simulations as described in the text. The insets show representative thin-layer cyclic voltammograms [v = 4 mV s^{-1} (a)] and cyclic voltammograms [v = 0.02 (b) and 1 (c) V s^{-1}].

Results

(a) Cyclic Voltammetric Studies. Both compounds **1** and **2** exhibit reversible cyclic voltammograms at fairly negative potentials ($E_{1/2}$ = −0.73 V for **1** and −0.88 V for **2** in THF), indicating electron richness. As expected, the W compound (**2**) is easier to oxidize than the Mo compound. Changing the solvent to CH_2Cl_2, MeCN, or acetone does not affect the reversibility nor the $E_{1/2}$ value for **2**, nor is any change observed upon changing the solvent to CH_2Cl_2 for **1**. On the other hand, **1** exhibits a semireversible system (−0.85 V) in MeCN, indicating a faster decomposition of $\mathbf{1}^+$ in this solvent (vide infra). The return scan shows a smaller intensity for the reduction wave of $\mathbf{1}^+$ and the appearance of a new reduction peak (−1.58 V). Faster scan rates resulted in an increased reversibility for the oxidation of **1**. Representative cyclic voltammograms at different scan rates are shown in the insets of Figure 3. The oxidation of **1** as a function of scan rate and concentration was investigated in both bulk (CV) and thin-layer (TLCV) cyclic voltammetry at 20 °C. The results yield useful information on the decomposi-

Table 3. Slope and Intercept with $E = E°$ of the Straight Lines Fitting the Anodic Peak Potentials at Low Scan Speeds (v in V s^{-1}) for the Oxidation of **1** in MeCN

	CV			TLCV		
log c^a	slope of $E_{p,a}$ (mV) vs log v	log v at $E = E°$ (log v_{CV_i})	log $k_{disp}{}^b$	slope of $E_{p,a}$ (mV) vs log v	log v at $E = E°$ (log v_{TLCV_i})	log $k_{deprot}{}^b$
−3.30		−3.20	3.65	52(4)	−2.1	2.49
−3.20	9(1)	−3.14	3.61	53(1)	−2.1	2.39
−3.19	14(5)	−3.11	3.63	56(5)	−1.95	2.53
−3.08	17(7)	−3.06	3.57	53(4)	−1.7	2.67
−3.05	22(5)	−3.05	3.55	49(1)	−1.9	2.44
−3.03	14(1)	−2.96	3.62	54(1)	−2.18	2.14

[a] $c = [\mathbf{1}]$ in mol L^{-1}. [b] See text (k in s^{-1} M^{-1}).

tion mechanism of the primary oxidation product $\mathbf{1}^+$ (see Discussion). In the region of scan rates where a distinctive return wave is observable (scan rate > 100 mV s^{-1}), both anodic and cathodic peak potentials are independent of scan speed and concentration. At lower scan rates, the anodic peak shifts to more negative potentials while the cathodic peak disappears. At constant concentration, the shift of the anodic peak potential is linear with respect to the logarithm of the scan rate in both CV and TLCV experiments. Figure 3 shows a representative study at $[\mathbf{1}] = 8.9 \times 10^{-4}$ M. Table 3 reports the slopes of these lines for all concentrations used in this study, as well as the value of log v at the intercept with the $E = E°$ horizontal line. The large errors on some of the slopes obtained in the CV study are the consequence of the limited range of scan rates (≤0.5 log unit) in the kinetic region.

At constant scan rate, the shift of the anodic peak potential is linear with respect to the logarithm of the concentration. The data were fit to straight lines, giving average slopes of −15 ± 3 mV per log unit for the CV data and −48 ± 7 mV per log unit for the TLCV data.

(b) Chemical Generation and Spectroscopic Characterizations of $\mathbf{1}^+$ and $\mathbf{2}^+$. The interaction of **1** and **2** with 1 equiv of Cp_2FePF_6 affords the corresponding cations, $\mathbf{1}^+$ and $\mathbf{2}^+$, respectively (see eq 1). Complex $\mathbf{1}^+$ can be generated in THF

$$Cp^*MH_3(dppe) + Cp_2FePF_6 \rightarrow [Cp^*MH_3(dppe)][PF_6] + Cp_2Fe \quad (1)$$

$$(M = Mo, \mathbf{1}^+PF_6^-; W, \mathbf{2}^+PF_6^-)$$

or CH_2Cl_2 at −80 °C and is indefinitely stable at this temperature. When the same reaction is carried out at room temperature, the formation of $\mathbf{1}^+$ still takes place, but this is followed by a relatively rapid decomposition ($t_{1/2}$ of a few minutes in both solvents). We shall examine this phenomenon and the nature of the decomposition product in more detail in section d. The EPR spectrum of $\mathbf{1}^+$ exhibits a triplet of quartets ($g = 1.989$, $a_P = 28.9$ G, $a_H = 11.8$ G; see Figure 1), consistent with coupling to three equivalent H and two equivalent P nuclei. The equivalence of the P and H hyperfine couplings in the EPR spectrum of $\mathbf{1}^+$ clearly indicates that fluxional processes are occurring. IR investigations show broad bands attributable to M−H stretching vibrations, which blue-shift upon oxidation (see Figure 2).

The chemical oxidation of **1**-d_3 in THF leads to the formation of $\mathbf{1}^+$-d_3, which is characterized by an EPR broad triplet at room temperature ($g = 1.991$, $a_P = 28.9$ G; see Figure 1), confirming the assignments made for the spectrum of $\mathbf{1}^+$. The triplet coupling is essentially identical with that observed for the corresponding trihydride complex, whereas the quartet coupling in $\mathbf{1}^+$ disappears on going to complex $\mathbf{1}^+$-d_3. IR investigations show a blue shift for the Mo−D vibrations upon oxidation of **1**-d_3 to $\mathbf{1}^+$-d_3 similar to that observed for the Mo−H vibrations of $\mathbf{1}^+$ relative to those of **1**. In addition, the expected isotope shift is observed upon H/D exchange on going from **1** to **1**-d_3 and from $\mathbf{1}^+$ to $\mathbf{1}^+$-d_3.

Compound $\mathbf{2}^+$ can be generated in THF, CH_2Cl_2, MeCN, or acetone at room temperature. It exhibits a broad triplet resonance in the EPR spectrum ($g = 2.017$; see Figure 1). Unlike complex $\mathbf{1}^+$, complex $\mathbf{2}^+$ is rather stable at room temperature in any of the aforementioned solvents, permitting its isolation in the solid state and the growth of single crystals suitable for X-ray analysis (vide infra). Cooling of the solution to −80 °C does not affect the line shape of the EPR signal. IR investigations for **2** and $\mathbf{2}^+$ also reveal a blue shift upon oxidation, as observed for the Mo analogue (see Figure 2). Oxidation of **2**-d_3 leads to $\mathbf{2}^+$-d_3, which better reveals the phosphorus coupling ($g = 2.022$, $a_P = 27.6$ G; see Figure 1). An IR investigation of these two complexes did not allow the identification of the W−D stretching vibrations (no visible change is detected in the IR spectrum upon oxidation), probably because these weak and broad bands are overshadowed by the other stronger bands.

(c) Chemical Oxidation of 1 in CH_3CN. The chemical oxidation of **1** with 1 equiv of Cp_2FePF_6 in MeCN provides very different results (see eq 2) relative to those of the same reaction in THF or CH_2Cl_2. An immediate and short-lasting (a

$$Cp^*MoH_3(dppe) \xrightarrow{Cp_2Fe^+} \{[Cp^*MoH_3(dppe)]^+\} \xrightarrow{MeCN} [Cp^*MoH_2(dppe)(MeCN)]^+ + [Cp^*MoH(dppe)(MeCN)_2]^{2+} \quad (2)$$

fast addition: ca. 17:83

slow addition (40 min): ca. 36:64

few seconds) H_2 evolution occurs, and no observable amount of $\mathbf{1}^+$ or any other paramagnetic species is shown by EPR investigation. The ^1H NMR analysis of the final solution revealed that two hydridic products, $[Cp^*MoH_2(MeCN)(dppe)]^+$ and *trans*-$[Cp^*MoH(dppe)(MeCN)_2]^{2+}$, are formed in a 17:83 ratio. Both products have previously been obtained by carrying out the protonation of **1** with HBF_4 in MeCN.[81] It is interesting to note, however, that the double protonation of **1** (or the protonation of $[Cp^*MoH_2(MeCN)(dppe)]^+$) gives rise to two different isomers of the dicationic product in a 3:1 ratio, the major product having a pseudo-trigonal prismatic structure and the minor, thermodynamically more stable isomer having a pseudo-octahedral structure.[81] The oxidation process reported here, on the other hand, gives *the thermodynamically more stable isomer selectively*. This demonstrates that the dicationic product cannot result from a proton transfer from $\mathbf{1}^+$ to either **1** or $[Cp^*MoH_2(MeCN)(dppe)]^+$ (see Discussion).

An additional oxidation experiment carried out under the same conditions, except that the 1 equiv of ferrocenium was admin-

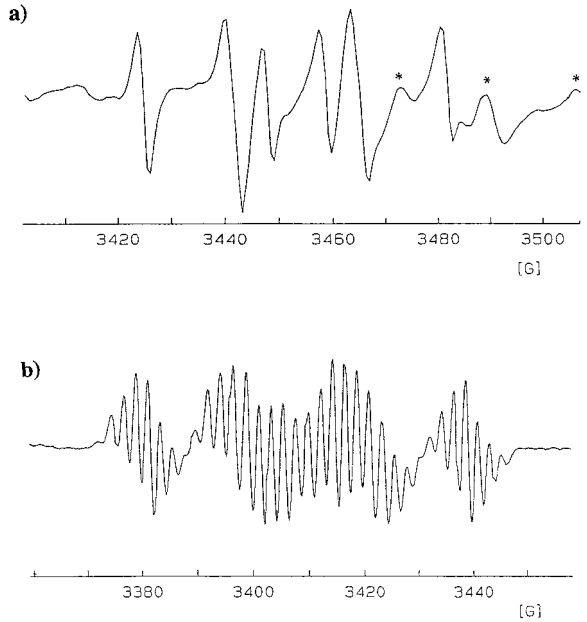

Figure 4. EPR spectrum of compound Cp*MoH(dppe)(PF_6). Solvent = CH_2Cl_2. (a) T = room temperature. (b) T = 0 °C. The peaks marked with an asterisk are due to an unknown impurity.

istered slowly over 40 min instead of all at once, gives the same two products of eq 2, but the dihydride/monohydride ratio is now 36:64. Once again, the monohydride complex is present in a single isomeric form, corresponding to the thermodynamically stable isomer.

(d) Decomposition of 1^+ in THF and CH_2Cl_2. Warming a THF or CH_2Cl_2 solution of $\mathbf{1}^+PF_6^-$ (generated at −80 °C, vide supra) to room temperature, or direct oxidation of **1** with Cp_2FePF_6 at room temperature in THF or CH_2Cl_2, causes decomposition of $\mathbf{1}^+$ with gas evolution. The decomposition was complete within a few minutes at room temperature, as shown by EPR monitoring. The nature of the gas as H_2 is confirmed by its resonance at δ 4.61 in the ^{1}H NMR spectrum, in comparison with an authentic sample. The reaction affords a new, highly air-sensitive compound (**3**), which is characterized by a doublet of triplets EPR resonance (g = 1.950, a_P = 16.5 G, a_H = 24.0 G; see Figure 4a), consistent with coupling to two equivalent P nuclei and one proton. The spectral parameters are identical whether the spectrum is taken in a THF, CH_2Cl_2, or MeCN solution. Notice that this product cannot be obtained directly by oxidation of **1** in MeCN (vide supra) but is rather stable in this solvent after it is formed. Solutions of **3** in MeCN decompose quite slowly ($t_{1/2} \approx 4$ h) to afford a mixture of the monohydride (thermodynamic isomer only) and dihydride products of eq 2, plus other noncharacterized, nonhydridic products.

Compound **3** has been isolated as a microcrystalline solid and is assigned the formula Cp*MoH(dppe)PF_6 on the basis of the EPR spectrum and the elemental composition (see eq 3).

$$\underset{\mathbf{1}^+PF_6^-}{[Cp^*MoH_3(dppe)][PF_6]} \xrightarrow{-H_2} \underset{\mathbf{3}}{Cp^*MoH(dppe)PF_6} \quad (3)$$

Elemental analysis indicates no solvent incorporation, and the IR spectra of batches of the compound recrystallized from THF or from MeCN are identical. On the basis of the nonexistence of half-sandwich compounds of Mo(III) with 15 valence electrons,[88] we propose that the PF_6^- anion is coordinated to the metal center in the solid state. Attempts to grow single crystals for this compound have been unsuccessful. The measured magnetic moment for solid **3** is 1.50 μ_B, close to the expected value for one unpaired electron. A spin doublet configuration is systematically observed for 17-electron half-sandwich complexes of Mo(III).[89]

Solutions of **3** in CH_2Cl_2 give rise to electrical conductivity (Λ_∞ = 35.4 S cm^2 mol^{-1}), in agreement with its formulation as a 1:1 salt;[90] thus, the PF_6^- anion is not coordinated to the metal in this solvent. The nonexistence of 15-electron half-sandwich Mo(III) complexes leads to the hypothesis that one loosely bound molecule of CH_2Cl_2 completes the coordination sphere in solution. This is confirmed by the EPR spectrum at 0 °C (Figure 4b). Each of the lines observed at room temperature splits, upon cooling of the solution to 0 °C, into a 1:2:3:4:3:2:1 septet, unambiguously indicating coupling to two equivalent Cl nuclei (^{35}Cl and ^{37}Cl, both $I = {}^3/_2$, similar gyromagnetic ratio, 100% total abundance). It is reasonable to propose that a single molecule of CH_2Cl_2 is coordinated to the metal in a chelating mode, as observed, for instance, in $Ag_2(CH_2Cl_2)_4Pd(OTeF_5)_4$ and in $[RuH(CH_2Cl_2)(CO)(PBu^t{}_2Me)_2][B(C_6H_3(CF_3)_2\text{-}3,5)_4]$,[91,92] rather than two separate molecules in a monodentate mode. Thus, all evidence points to the formulation of **3** in CH_2Cl_2 as [Cp*MoH(dppe)(η^2-Cl_2CH_2)]$^+PF_6^-$, having a 19-electron configuration for the metal valence shell. The inability to observe the Cl coupling at room temperature must be ascribed to a fast exchange between the loosely bound CH_2Cl_2 ligand and the free solvent. Cooling the THF and MeCN solutions did not result in any change in the EPR spectrum. In particular, no coupling to the ^{14}N (I = 1, 100%) nucleus/nuclei was observable in MeCN down to −45 °C. On the basis of the results obtained in CH_2Cl_2, it is reasonable to assume that the complex also coordinates a solvent molecule when dissolved in THF or MeCN, since the latter Lewis bases have stronger coordinating properties than CH_2Cl_2. The most likely structure in these cases is a four-legged piano stool for [Cp*MoH(dppe)(S)]$^+$ (S = THF or MeCN) with a 17-electron configuration at the metal center.

This formulation is in agreement with the electrochemical studies. Compound 3 shows an irreversible oxidation wave at 1 V s^{-1}, whose peak potential depends on the nature of the solvent: 0.719 V in THF, 0.597 V in CH_2Cl_2, and 0.504 V in MeCN. A reverse reduction wave is not observed, even when carrying out the experiments at 100 V s^{-1}. Although these potential shifts should be taken with some caution, they are too large to be attributed solely to differences (if any) in follow-up chemical processes and to a solvent dependence of the ferrocene redox process. Therefore, the anodic peak potential can be taken as a qualitative measure of the electron richness at the metal. The donor power of the three solvents in the order MeCN > THF > CH_2Cl_2 should lead to anodic peak potentials in the reverse order. However, the observed order is different (MeCN < CH_2Cl_2 < THF). The unexpected CH_2Cl_2/THF reversal may be reconciled with the proposed chelating coordination mode of dichloromethane and with monocoordination for THF. In other words, dichloromethane is effectively a better electron donor, by virtue of its bidentate coordination mode, than a single molecule of THF.

(88) Abugideiri, F.; Keogh, D. W.; Kraatz, H.-B.; Poli, R.; Pearson, W. *J. Organomet. Chem.* **1995**, *488*, 29−38.
(89) Poli, R. *J. Coord. Chem. B* **1993**, *29*, 121−173.
(90) Burgess, J. *Ions in Solution: Basic Principles of Chemical Interactions*; Wiley: New York, 1988; p 187.
(91) Colsman, M. R.; Newbound, T. D.; Marschall, L. J.; Noirot, M. D.; Miller, M. M.; Wulfsberg, G. P.; Frye, J. S.; Anderson, O. P.; Strauss, S. H. *J. Am. Chem. Soc.* **1990**, *112*, 2349−2362.
(92) Huang, D.; Huffman, J. C.; Bollinger, J. C.; Eisenstein, O.; Caulton, K. G. *J. Am. Chem. Soc.* **1997**, *119*, 7398−7399.

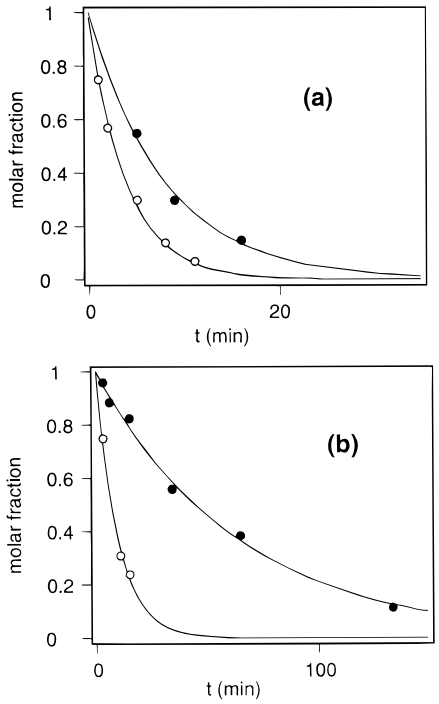

Figure 5. Decay from the EPR monitoring experiments of the relative concentration of (a) $\mathbf{1}^+$ (●) and $\mathbf{1}^+$-d_3 (○) in CH_2Cl_2 at 0 °C and (b) $\mathbf{1}^+$ in THF at 0 °C (●) and 10 °C (○).

The decomposition of $\mathbf{1}^+$ was investigated kinetically by EPR monitorning in both THF and CH_2Cl_2 below room temperature. The extensive overlap of the EPR signals required the determination of the relative concentrations of residual $\mathbf{1}^+$ and product by signal subtraction. The quality of the data was not sufficient to obtain accurate double integrals, but an estimate of the relative concentration at each time was obtained by comparison of the subtracted spectrum with the initial spectrum multiplied by a coefficient. The resulting data show the expected first-order decay (see Figure 5) in all cases. The decay is much faster in CH_2Cl_2 ($k = 0.125(6)$ min^{-1} at 0 °C) relative to that in THF ($k = 0.016(1)$ min^{-1} at 0 °C and 0.100(3) min^{-1} at 10 °C).

As expected from the behavior of the hydride analogue, $\mathbf{1}^+$-PF_6^--d_3 decomposes in THF at room temperature to afford Cp*MoD(dppe)PF_6 (**3**-d). The EPR spectrum of **3**-d at room temperature allows the observation of the deuterium coupling as 1:1:1 triplets ($a_D = 4.0$ G), which is related to the H coupling of **3** by a measured a_H/a_D ratio of 6.0, close to the theoretical value of 6.5. The EPR monitoring of this transformation in CH_2Cl_2 at 0 °C and the subsequent data analysis as outlined above for the trihydride analogue yielded the data illustrated in Figure 5a and a first-order rate constant of 0.25(1) min^{-1}. Therefore, the decay of the oxidized trihydride complex shows an *inverse* isotope effect, $k_H/k_D = 0.50(3)$.

(e) Structural Characterizations. A single-crystal X-ray investigation of $\mathbf{2}^+PF_6^-$ permitted the location and refinement of the three hydride ligands (see Figure 6). Neglecting the hydrogen positions, the geometry of $\mathbf{2}^+$ is almost identical with that of complex $[Cp^*WH_4(dppe)]^+$ ($[\mathbf{2}\text{-H}]^+$), namely the protonation product of **2**. This tetrahydrido cation had been previously characterized by X-ray diffraction as the BF_4^- salt.[81] The major difference consists of a small displacement (0.025(8) Å, as opposed to 0.002(9) Å in the tetrahydrido complex) of the W atom from the plane defined by CNT, P(1) and P(2), toward the side of the molecule occupied by H2 and H3 (see Figure 6). There are also small differences between the CNT−W−P1 and CNT−W−P2 angles for $\mathbf{2}^+$ and $[\mathbf{2}\text{-H}]^+$ (while CNT−W−P1 is larger by 1.6(2)° for $[\mathbf{2}\text{-H}]^+$, CNT−W−P2 is larger by 1.4(2)° for $\mathbf{2}^+$). The W−P and W−Cp* bond distances (see Table 2) are very similar for $\mathbf{2}^+$ and $[\mathbf{2}\text{-H}]^+$, suggesting that the replacement of a W−H bond with a singly occupied W orbital does not greatly affect the effective metal charge (i.e., the W−H bond is highly covalent). The geometry of $\mathbf{2}^+$ is intermediate between **I** (a pseudo-trigonal prism) and **II** (a pseudo-octahedron), i.e., the ideal geometries adopted by the isoelectronic d^2 complexes **1** and *trans*-octahedral $[Cp^*MoH(dppe)(MeCN)_2]^{2+}$ (MeCN occupies the two trans H positions), respectively.[81]

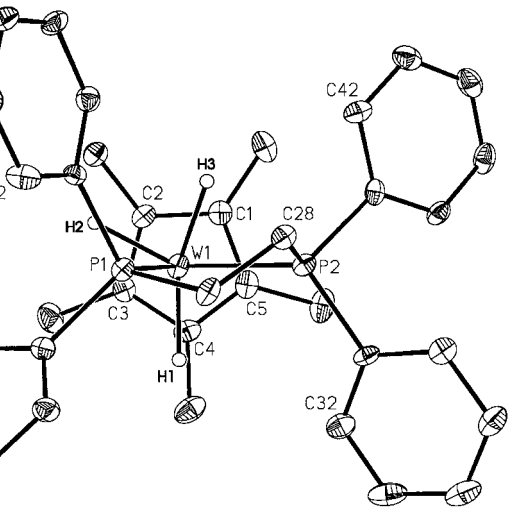

Figure 6. ORTEP view of the molecular geometry for $\mathbf{2}^+$. Ellipsoids are drawn at the 30% probability level.

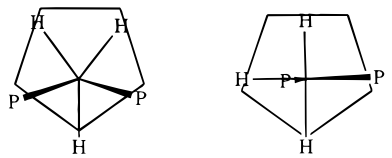

I **II**

There was some concern, given the remarkable structural similarities between the [Cp*W(dppe)] moieties in complexes $\mathbf{2}^+$ and $[\mathbf{2}\text{-H}]^+$, that the crystal examined could correspond to compound $[Cp^*WH_4(dppe)]PF_6$. This possibility seems excluded by the simple observation that the crystal of $\mathbf{2}^+PF_6^-$ used for the X-ray experiment is orange, while that of $[Cp^*MoH_3(dppe)][PF_6]^+BF_4^-$ is colorless. Nevertheless, in the search for additional evidence, the tetrahydride cation has also been crystallized with the PF_6^- counterion, and an X-ray structure has been determined on a genuine (colorless) crystal of $[\mathbf{2}\text{-H}]^+PF_6^-$. The variations of the metric parameters of the [Cp*W(dppe)] moiety are rather small (see Table 2), but the differences in unit cell parameters (Table 1) are sufficient to establish that the two crystals relate to two similar but different compounds. Furthermore, dissolution of crystals from the same batch used for the X-ray investigation showed no NMR signal attributable to $[\mathbf{2}\text{-H}]^+$ for the sample of $\mathbf{2}^+$ and no EPR signal attributable to $\mathbf{2}^+$ for the sample of $[\mathbf{2}\text{-H}]^+$.

(f) DFT Calculations. Calculations on the $[CpWH_x(H_2PCH_2CH_2PH_2)]^{n+}$ ($x = 3, 2$; $n = 0, 1$) model systems were carried out with the following objectives in mind. A full geometry optimization starting from different ideal configurations could reproduce the somewhat bizarre structural preference for both

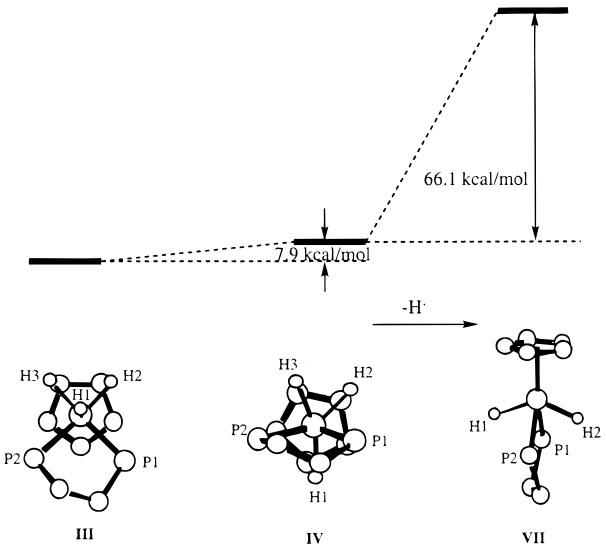

Figure 7. B3LYP/LANL2DZ-optimized geometries and relative energies for $CpWH_3(H_2PCH_2CH_2PH_2)$ and $CpWH_2(H_2PCH_2CH_2PH_2)$ + H.

the neutral and the cationic complexes. Complex **1**, in fact, was shown to adopt a pseudo-trigonal prismatic geometry which is unprecedented for compounds with the $CpMX_3L_2$ stoichiometry.[81,93] For this purpose, the $H_2PCH_2CH_2PH_2$ model rather than the more typical $(PH_3)_2$ system was chosen to replace the dppe ligand. In addition, a comparison between the energy changes for eqs 4 and 5 could provide information on the M−H bond strength dependence on the metal oxidation state.

$$CpWH_3(H_2PCH_2CH_2PH_2) \rightarrow CpWH_2(H_2PCH_2CH_2PH_2) + H \quad (4)$$

$$[CpWH_3(H_2PCH_2CH_2PH_2)]^+ \rightarrow [CpWH_2(H_2PCH_2CH_2PH_2)]^+ + H \quad (5)$$

All geometry optimizations were carried out with a standard LANL2DZ basis set (basis I) for all atoms. Single-point calculations were then carried out at these optimized geometries by using an augmented basis set (basis II) with triple-ζ functions for the hydridic hydrogen atoms. The effect of introducing a third contraction for the description of the hydride atomic orbital is a lowering of the total energy by a few kilocalories per mole for each system. However, the relative energies at the basis II level do not differ from those at the basis I level by more than 0.3 kcal/mol.

The results of the geometry optimizations are summarized in Figures 7 and 8. The global minimum for the neutral trihydride complex corresponds to a pseudo-octahedral structure (structure **III** in Figure 7), while the next most favored structure (**IV**) corresponds to the experimentally observed (for **1**) pseudo-trigonal prismatic structure. The discrepancy between the theoretical prediction and the experimental result is probably due to the steric repulsion between the Cp* and the dppe ligands. The calculated bond distances and angles for the W model system **IV** are in good agreement with those observed for the Mo system **1** (the calculated geometrical parameters of systems **III**−**IX** have been deposited as Supporting Information). The calculated hydrogen positions are remarkably close to those determined by the single-crystal X-ray analysis, although the latter are subject to large uncertainties. Thus, the results of our calculations provide support to the geometry proposed on the basis of X-ray data for **1** and, at the same time, suggest that **2** should adopt a structure identical with that of **1**. A calculation based on a *cis-mer* pseudo-octahedral starting geometry, as experimentally observed for the trichloride complexes $CpMoCl_3$(dppe) and $CpMoCl_3$(dmpe),[94,95] led again to **IV**, showing that there is an *electronic preference* for the pseudo-trigonal prismatic geometry. This preference must be related to the geometrical constraint of the chelating ligand, since the $CpMoH_3(PMe_2Ph)_2$ complex with two monodentate phosphorus ligands was experimentally found to adopt a *mer-trans* pseudo-octahedral structure.[96]

The global energy minimum for the cationic system is obtained for a geometry (**VI** in Figure 8) which corresponds remarkably well to that experimentally determined for $\mathbf{2}^+$ (compare Figure 8 with Figure 6). Once again, the remarkable closeness of the hydride positions calculated by theory (see Supporting Information) to those obtained from the X-ray data gives stronger confidence in the correctness of the experimental result. Starting from the geometry of the neutral global minimum, an *eq*,*eq* octahedral local minimum (structure V in Figure 8) which is only 0.8 kcal/mol higher in energy than the global minimum (0.2 kcal/mol at the basis II level) was obtained. Considering the Cp*-dppe steric repulsion (greater in the *eq*,*eq* pseudo-octahedral structure), the computational result provides an even stronger justification for the adoption of the observed structure by complex $\mathbf{2}^+$.

A comparison of the $[CpWH_3(H_2PCH_2CH_2PH_2)]^{n+}$ (n = 0, **IV**; 1, **VI**) optimized structures shows that the W−H distances become *shorter* upon oxidation (average −0.010 Å), while the W−P and W−CNT distances become *longer* (+0.085 and +0.007 Å, respectively). While the shortening of the W−H distances is as expected on the basis of a contraction of the W atomic radius upon oxidation, the lengthening of the W−P and W−CNT distances indicates correspondingly weaker interactions in the oxidized complex. Variations of this kind have been noted before and attributed to a weakening of the M−P π and M−Cp δ back-bonding components, respectively.[97−100]

The W−H bond strengthening upon oxidation is further confirmed by the calculation of the bond dissociation energies according to the processes of eqs 3 and 4. For the neutral system, each of the three inequivalent hydride ligands H1, H2, and H3 was removed as a neutral H atom from structure **IV** to give a different 17-electron $CpWH_2(H_2PCH_2CH_2PH_2)$. The three resulting fragments were calculated at their fixed geometries, giving rise to energy differences (also called *bond energy terms*)[101] of 77.3, 72.7, and 79.6 kcal/mol (77.5, 72.7, and 79.5 kcal/mol at the basis II level). Subsequently, the lowest energy geometry was allowed to relax, giving the fully optimized doublet $CpWH_2(H_2PCH_2CH_2PH_2)$ geometry shown (**VII**) in Figure 7, which corresponds to the geometry experimentally observed for complex Cp^*MoCl_2(dppe).[102] The cis isomer for

(93) Fettinger, J. C.; Pleune, B.; Poli, R. *J. Am. Chem. Soc.* **1996**, *118*, 4906−4907.
(94) Stärker, K.; Curtis, M. D. *Inorg. Chem.* **1985**, *24*, 3006−3010.
(95) Owens, B. E.; Poli, R. *Inorg. Chim. Acta* **1991**, *179*, 229−237.
(96) Abugideiri, F.; Fettinger, J. C.; Pleune, B.; Poli, R.; Bayse, C. A.; Hall, M. B. *Organometallics* **1997**, *16*, 1179−1185.
(97) Orpen, A. G.; Connelly, N. G. *Organometallics* **1990**, *9*, 1206−1210.
(98) Orpen, A. G.; Connelly, N. G. *J. Chem. Soc., Chem. Commun.* **1985**, 1310−1311.
(99) Krueger, S. T.; Poli, R.; Rheingold, A. L.; Staley, D. L. *Inorg. Chem.* **1989**, *28*, 4599−4607.
(100) Keogh, D. W.; Poli, R. *J. Chem. Soc., Dalton Trans.* **1997**, 3325−3333.
(101) Martinho Simões, J. A.; Beauchamp, J. L. *Chem. Rev.* **1990**, *90*, 629−688.

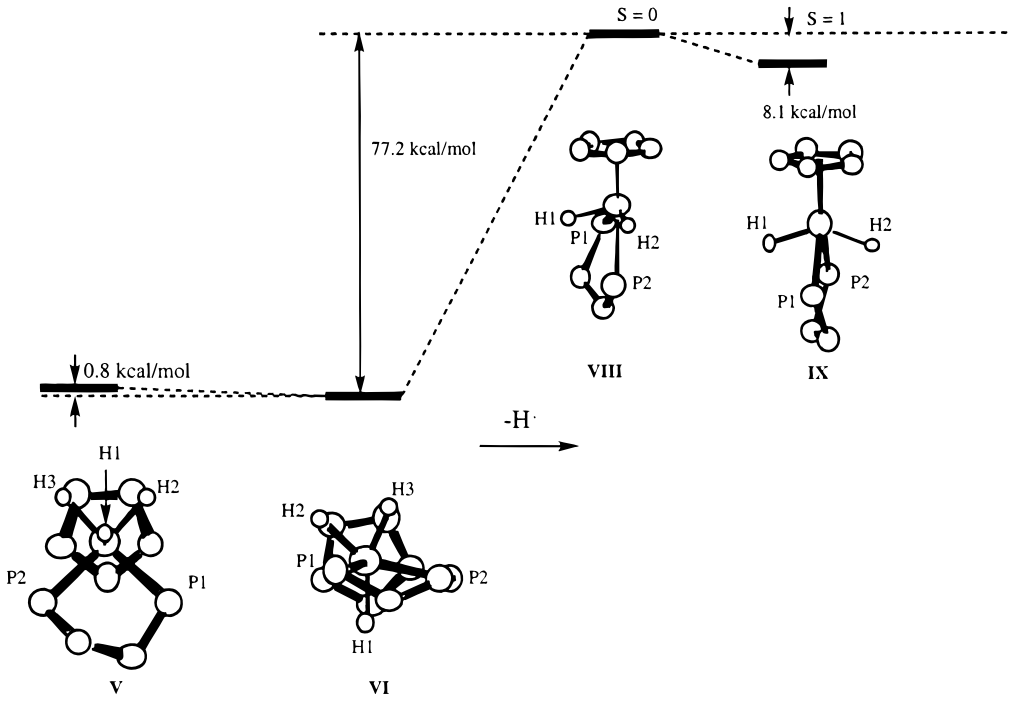

Figure 8. B3LYP/LANL2DZ-optimized geometries and energies for $[CpWH_3(H_2PCH_2CH_2PH_2)]^+$ and $[CpWH_2(H_2PCH_2CH_2PH_2)]^+ + H$.

the dihydride system was optimized to a local minimum 2.5 kcal/mol higher (3.0 kcal/mol at the basis II level) than the trans isomer.

An analogous procedure was repeated for the cationic complex (see Figure 8), the 16-electron dihydrido complex $[CpWH_2(H_2PCH_2CH_2PH_2)]^+$ being calculated in both singlet (**VIII**) and triplet (**IX**) spin states, the latter yielding a more stable structure. It is interesting to note that the optimized triplet geometry is a four-legged piano stool, qualitatively similar to those experimentally observed by X-ray crystallography for the spin triplet Cp^*MoCl_3L ($L = PMe_3$, $PMePh_2$) and $[CpMoCl_2(PMe_3)_2]^+$ complexes.[99,103] The optimized singlet geometry, on the other hand, is better viewed as a pseudo-octahedral structure with a missing equatorial position. In this structure, the chelating $H_2PCH_2CH_2PH_2$ ligand occupies an equatorial and the axial position, as experimentally observed for $CpMoCl_3(dmpe)$.[95] Other geometric arrangements gave higher energy local minima for both singlet and triplet configurations. Similarly to the trihydride system mentioned above, the dihydride system also shows a shortening of the W−H distances and a lengthening of the W−P and W−CNT distances upon oxidation.

As shown by the calculations, the BDE for the W−H bonds (with respect to the relaxed dihydride geometry) increases from 66.1 kcal/mol for the neutral trihydride system to 69.1 kcal/mol for the cationic complex (relative to the triplet ground state). This increase is paralleled, as expected, by an increase of overlap population for the three W−H bonds: the values increase from 0.232 to 0.258 for W−H1, from 0.227 to 0.233 for W−H2, and from 0.241 to 0.245 for W−H3, respectively.

A normal-mode analysis was carried out on the $[CpWH_3(H_2PCH_2CH_2PH_2)]^{n+}$ optimized geometries that correspond to the experimentally observed structures for **1** and $\mathbf{2}^+$. The calculated normal modes of vibration for the $[WH_3]^{n+}$ moiety reproduce the experimentally observed increase of frequency upon oxidation. The calculated frequencies (relative intensities in parentheses) are 1828 (1), 1862 (0.79), and 1951 (0.30) cm^{-1} for $n = 0$ and 1885 (0.75), 1920 (1), and 1960 (0.33) cm^{-1} for $n = 1$. The frequencies, relative intensities, and normal modes are also shown in Figure 2b, in comparison with the experimental IR spectra. The correspondence between calculated and experimental spectra is quite acceptable. This agreement confirms the strengthening of the W−H bonds upon oxidation, which is independently indicated by the bond shortening and BDE increase.

Discussion

(a) M−H Bond Strength. The W−H bond strengthening upon oxidation of **1** and **2** is clearly indicated by three independent experimental and/or computational results: (i) the shortening of all W−H bonds calculated for the $[CpWH_3(H_2PCH_2CH_2PH_2)]^{n+}$ system; (ii) the increase of the calculated BDE for the same model system; and (iii) the blue shift of the Mo−H(D) and W−H stretching vibrations upon oxidation of **1** (**1**-d_3) and **2**, the latter being reproduced by the calculations on the model systems. From simple theory, the vibrational frequency correlates directly with the bond energy and inversely with the bond length.[104] Although exceptions to this rule have been presented for bonds that contain multiple components (e.g., ligand−metal σ bonding + π back-bonding), whereupon stronger bonds are occasionally found *not* to be the shortest,[105] a similarly unusual behavior is not expected for a bond as simple as a terminal M−H bond.

This M−H bond strengthening upon oxidation is a novel finding in transition metal hydride chemistry. Unfortunately, most 17-electron hydride complexes are too unstable for IR studies. IR studies of $[Cp^*FeH(dppe)]^+$, $[WH_2Cl_2(PMe_3)_4]^+$, and their respective neutral precursors indicated either no change or a slight *red shift* in the spectra upon oxidation.[8,9] The use of thermodynamic cycles involving pK_a and electrochemical

(102) Fettinger, J. C.; Keogh, D. W.; Pleune, B.; Poli, R. *Inorg. Chim. Acta* **1997**, *261*, 1−5.

(103) Abugideiri, F.; Gordon, J. C.; Poli, R.; Owens-Waltermire, B. E.; Rheingold, A. L. *Organometallics* **1993**, *12*, 1575−1582.

(104) *Infrared and Raman Spectroscopy: Methods and Applications*; Schrader, B., Ed.; VCH: Weinheim, 1995; p 693.

(105) Ernst, R. D.; Freeman, J. W.; Stahl, L.; Wilson, D. R.; Arif, A. M.; Nuber, B.; Ziegler, M. L. *J. Am. Chem. Soc.* **1995**, *117*, 5075−5081.

Scheme 1

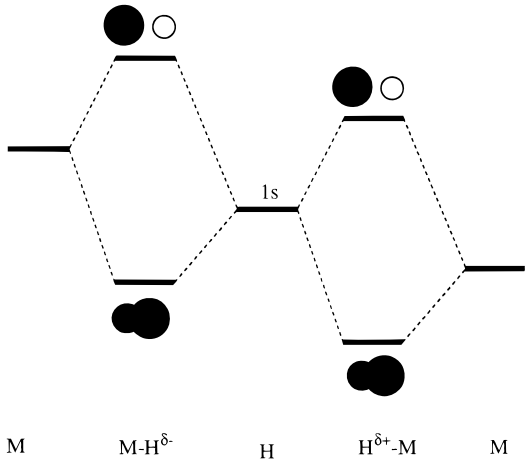

measurements led to the deduction of a M−H bond *weakening* by 8−12 kcal/mol upon one-electron oxidation for compounds $CpCrH(CO)_2L$ (L = $P(OMe_3)_3$, PPh_3, PEt_3), $Cp^*CrH(CO)_3$, $TpMH(CO)_3$, $Tp^*MH(CO)_3$ (M = Cr, Mo, W), and $Cp^*FeH(dppe)$.[72,106,107]

To visualize the expected effect of oxidation on the M−H bond strength, let us qualitatively analyze the M−H bond as having a covalent and an ionic component, according to Pauling. Let us first focus on the covalent component. A M−H$^{\delta-}$ bond polarity corresponds to a situation where the M frontier orbital is higher in energy than the H frontier orbital (1s) (see Scheme 1, left). An increase of formal positive charge on the metal center (such as, for instance, following an oxidation process) has two main effects: (i) it lowers the energy of the metal-based frontier orbital used for the M−H interaction and (ii) it contracts the metal orbitals. The first effect has a positive consequence on the M−H bond strength if the frontier orbital ends up closer in energy to the H 1s orbital. An excessive energy lowering, on the other hand, would weaken the covalent interaction. The second effect has two consequences: it lowers the overlap between the frontier orbitals of M and H, weakening the interaction, but it also reduces the metal radius, allowing the H atom to approach the metal at a closer distance. All in all, the orbital contraction may provide a positive contribution to bond strengthening. The DFT calculations on the $[CpWH_3(H_2PCH_2CH_2PH_2)]^{n+}$ systems show an increase of M−H overlap population upon oxidation (see Results). For a system having a M−H$^{\delta+}$ bond polarity (Scheme 1, right), the increase of formal charge on the metal may have again a positive effect on the orbital overlap as a consequence of the radius contraction, but the energy separation between the frontier orbitals becomes larger, decreasing the strength of the interaction.

Concerning the ionic component of the M−H bond, for a metal-based HOMO (a typical situation for d^n configurations with $n > 0$), oxidation results in an increased effective positive charge (or a decreased negative charge) for the metal, as well as an increased "group electronegativity" for the M fragment (viz., the metal with all its ligands except the hydride). The latter effect leads to a greater draw of electron density from the H ligand, reducing its effective negative charge or increasing its effective positive charge. The two effects combine to yield any possible result (strengthening or weakening of the ionic interaction) for a M−H$^{\delta-}$ bond system, including an inversion

Scheme 2

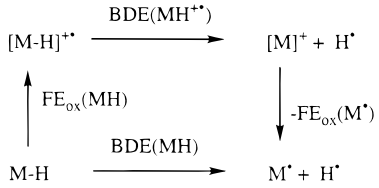

$$BDE(MH)\text{-}BDE(MH^{+\bullet}) = F[E_{ox}(MH)\text{-}E_{ox}(M^\bullet)]$$

of polarity. For a M−H$^{\delta+}$ system, oxidation should definitely lead to a weakening of the ionic component. Notice, however, that the sharp acidity increase following oxidation of hydride complexes[108] is not, per se, an indication of M−H$^{\delta+}$ bond polarity. Experimental and theoretical studies of charge distribution in low-valent, carbonyl-based transition metal hydrides always indicate a M−H$^{\delta-}$ bond polarization, even for highly acidic complexes.[109−111] For instance, XPS studies lead to the estimation of a hydride formal charge of −0.3, −0.8, and −0.75 for $H_2Fe(CO)_4$, $HMn(CO)_5$, and $HCo(CO)_4$, respectively.[109]

The net effect of oxidation on the M−H bond strength may thus be either a strengthening or a weakening, although strengthening is expected for M−H$^{\delta-}$ systems with very electron-rich fragments (high-energy M frontier orbital) and when the bonding energetics is dominated by the covalent component. Compounds **1** and **2** contain ligands that have low electronegativities, are strong electron donors, and do not have strong π-accepting capabilities. Consequently, the Cp*M(dppe) (M = Mo, W) fragments have a low "group electronegativity".

One final consideration may be made on the basis of the thermodynamic cycle (Scheme 2) that was introduced by Tilset et al.[72,106,107] to estimate bond strength variations on the basis of electrochemical data. According to this cycle, a M−H bond weakening is associated with systems for which the oxidation of M$^\bullet$ occurs at a less positive potential (easier oxidation) relative to that for the oxidation of MH. We want to offer a word of caution about the use of this cycle. The 16-electron $[M]^+$ species (and to a lesser and variable extent also the 17-electron M$^\bullet$ and $[MH]^{\bullet+}$ species) is highly likely to establish strong interactions with the polar solvent or with the supporting electrolyte used for the electrochemical measurements, skewing the calculation toward the result of a MH bond weakening following oxidation. In other words, the calculated difference $F[E_{ox}(MH) - E_{ox}(M^\bullet)]$ should also reflect variations in the extent of metal−medium interactions. For our system, we cannot experimentally carry out this study because of the unavailability of $Cp^*MH_2(dppe)$ (M = Mo, W). The DFT calculations, however, yield a ΔE of −3.0 kcal/mol for reaction 6. Assuming negligible $\Delta(PV)$ and

$$CpWH_3(H_2PCH_2CH_2PH_2) + [CpWH_2(H_2PCH_2CH_2PH_2)]^+ \rightarrow [CpWH_3(H_2PCH_2CH_2PH_2)]^+ + CpWH_2(H_2PCH_2CH_2PH_2) \quad (6)$$

$T\Delta S$ factors, this corresponds to the free energy change ΔG, allowing us to calculate a less positive potential (by 0.13 V)

(106) Skagestad, V.; Tilset, M. *J. Am. Chem. Soc.* **1993**, *115*, 5077−5083.

(107) Tilset, M.; Hamon, J.-R.; Hamon, P. *J. Chem. Soc., Chem. Commun.* **1998**, 765−766.

(108) Ryan, O. B.; Tilset, M.; Parker, V. D. *J. Am. Chem. Soc.* **1990**, *112*, 2618−2626.

(109) Chen, H.-W.; Jolly, W. L.; Kopf, J.; Lee, T. H. *J. Am. Chem. Soc.* **1979**, *101*, 2607−2610.

(110) Sweany, R. L. In *Transition Metal Hydrides*; Dedieu, A., Ed.; VCH: 1992; pp 65−101.

(111) Bauschlicher, C. W., Jr.; Langhoff, S. R. In *Transition Metal Hydrides*; Dedieu, A., Ed.; VCH: 1992; pp 103−126.

Scheme 3

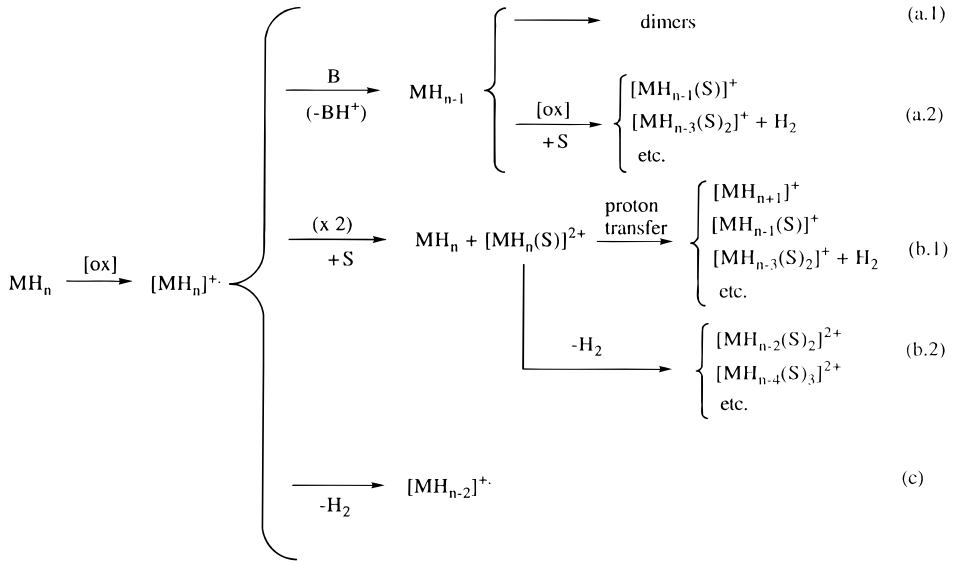

for the $[CpWH_3(H_2PCH_2CH_2PH_2)]^{0/+}$ couple relative to that for the $[CpWH_2(H_2PCH_2CH_2PH_2)]^{0/+}$ couple, in accord with the bond strengthening picture. This calculated potential shift refers, of course, to gas-phase, isolated species and is not contaminated by interactions with an electrochemical medium. It is to be observed that eq 6 is nothing other than the difference between eqs 4 and 5.

(b) Hydride Scrambling Process. As shown in the Results section, the equivalence of the P and H hyperfine couplings in the EPR spectrum of $\mathbf{1}^+$ clearly indicates that fluxional processes are occurring, averaging both the H and P ligands in the system. Due to the broadness of the EPR signal, a similar fluxional process is not unequivocally identified for complexes $\mathbf{2}^+$ and $\mathbf{2}^+$-d_3 (see Figure 1). As shown by the X-ray investigation and backed up by the DFT geometry optimization, the structure of $\mathbf{2}^+$ is pseudo-octahedral, with a significant twist toward a pseudo-trigonal prismatic geometry. The structure of $\mathbf{1}^+$ can be reasonably assumed to be identical to that of $\mathbf{2}^+$. Thus, it is very likely that the fluxional process involves the fast interconversion of pseudo-octahedral and pseudo-trigonal prismatic structures in solution, involving a pseudo-Bailar twist. The same scrambling mechanism was previously proposed for the precursor complexes **1** and **2**.[81,96]

(c) Stability of $[Cp^*MH_3(dppe)]^+$ (M = Mo, W). Stable and unambiguous examples of paramagnetic transition metal polyhydride complexes are exceedingly rare. Structurally characterized examples are $TaCl_2H_2L_4$[7] and $[WCl_2H_2(PMe_3)_4]^+$.[8] A factor involved in the stability of these and other paramagnetic polyhydride species may be the presence of π-donor ligands such as Cl which are capable of establishing interactions with the half-filled metal-based HOMO. The stabilizing effect of halide for hydride substitution has been pointed out by Kochi et al. in a study involving the lifetimes of various Cp_2WX_2 radical cations (X = H, Cl).[58] Complexes $\mathbf{1}^+$ and $\mathbf{2}^+$, on the other hand, do not have π-donor-stabilizing ligands; thus, other reasons must be found for their relative stability.

Since one of the principal decomposition pathways for 17-electron monohydride complexes is deprotonation by virtue of the increased acidity relative to that of the 18-electron precursors,[108] an increased stability may be expected through the use of donor ligands via a buffering effect of this acidity. At the same time, donor ligands render the 18-electron precursor more easily oxidizable, as experimentally verified for several systems, such as the $CpRe(PAr_3)_2H_2$ (Ar = *p*-C_6H_4X; X = H, Me, F, OMe)[63] and $Cp^*Ru(L_2)H$ (L_2 = dppm, dppp, $(PPh_3)_2$, $(PMePh_2)_2$, $(PMe_2Ph)_2$, $(PMe_3)_2$)[43] series. A qualitative correlation between oxidation potential and stability is, indeed, typically observed. The substitution of a more electron-rich metal for one less so will also result in a similar effect on the oxidation potential of the complex and a dampening of the hydride acidity.[106,108] However, the 18-electron hydride precursor is a possible base for the deprotonation pathway of decomposition of its own oxidation product, and its basicity is raised by the same factors that lower the acidity of the radical cation. Thus, the overall proton-transfer thermodynamics should remain approximately unaffected. The stabilization of 17-electron hydride complexes by donor ligands must be more a kinetic than a thermodynamic phenomenon. A lowering of the *kinetic* acidity as a result of steric protection has also been invoked to explain the stability of complexes $[Cp^*FeH(dppe)]^+$ and $[CpMoH(PMe_3)_3]^+$.[9,112]

When proton transfer is kinetically slow, the starting 18-electron hydride can be completely consumed by the oxidant, and the decomposition mechanism by proton transfer can be eliminated if sufficiently strong external bases are absent. Under these conditions, the radical complex can still decompose by a disproportionation mechanism.[57,75,112] Steric protection, however, should also slow a decomposition process by disproportionation, since this is usually initiated by the coordination of a donor molecule to the 17-electron complex. These simple arguments rationalize well the observed stability of complexes $\mathbf{1}^+$ and $\mathbf{2}^+$. In fact, complex $\mathbf{1}^+$ *does not decompose by disproportionation*, but rather by H_2 reductive elimination (except in acetonitrile). A discussion of the decomposition mechanism and a reason for the faster decomposition of the Mo complex are presented in the following sections.

(d) Decomposition Mechanisms for Paramagnetic Polyhydride Species: An Introduction. Mechanistic studies of the decomposition of paramagnetic polyhydride systems are less common than those of the corresponding monohydride systems. Based on the available literature, the current knowledge may be summarized as shown in Scheme 3. Deprotonation (by action of either the residual unoxidized starting material or another external base, paths a) leads to collapse to dimeric products

(112) Fettinger, J. C.; Kraatz, H.-B.; Poli, R.; Quadrelli, E. A.; Torralba, R. C. *Organometallics* **1998**, *17*, 5767−5775.

Scheme 4

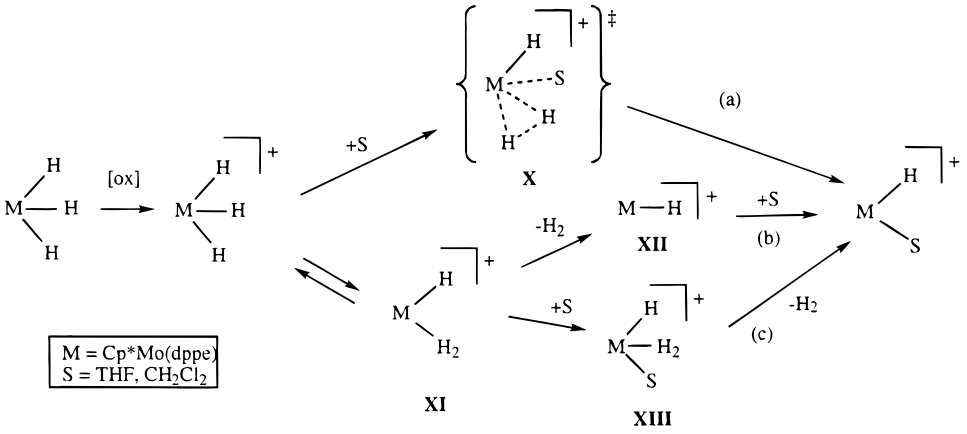

(path a.1) or to further oxidization (path a.2). It seems that the former possibility is favored only for relatively unhindered systems that lead to the formation of strong metal−metal interactions, e.g., Cp_2WH_2,[58] $(C_5H_4SiMe_3)_2NbH_3$,[68] and $[ReH_6(PMePh_2)_2]^-$.[61] The alternative product of further oxidation (path a.2) is stabilized by solvent coordination. In addition, under the influence of the reduced electron density following oxidation, one or more pairs of hydride ligands may collapse to dihydrogen ligands and be replaced by additional solvent molecules, producing a class of products of general formula $[MH_{n+1-2k}(S)_k]^+$. This path of decomposition has been proven or inferred (from supporting protonation studies) for a few polyhydride complexes, e.g., $IrH_3(PMe_2Ph)_3$,[71] $Cp^*RuH_3(PPh_3)$,[76] and $OsH_6(PPr^i_3)_2$.[113]

The disproportionation mechanism (paths b) is much less common and has been unambiguously shown, to the best of our knowledge, only for monohydride species.[57,75,112] On the basis of the scheme established for the monohydride species, the disproportionation products MH_n and $[MH_n(S)]^{2+}$ should rearrange by proton transfer to afford a mixture of $[MH_{n+1}]^+$ and $[MH_{n-1}(S)]^+$. Donor solvents may again induce loss of H_2 as indicated in Scheme 3 (path b.1). An additional possibility, however, is reductive elimination of H_2 at the level of the dicationic intermediate $[MH_n(S)]^{2+}$ (path b.2). This would lead to an entirely new series of products that are characterized by a double positive charge and by the same parity for the number of hydride ligands as the starting material, i.e., complexes having the general formula $[MH_{n-2k}(S)_{k+1}]^{2+}$. This latter pathway is not available for the disproportionation of monohydride complexes and thus represents an important chemical probe for the decomposition mechanism. Care, however, should be excercised because the $[MH_{n-2k}(S)_{k+1}]^{2+}$ complexes may also be obtained by path a.2 if the product $[MH_{n+1-2k}(S)_k]^+$ (rather than the starting material or another external base) serves as proton acceptor (B). Notably, the previously reported acidolysis of **1** in MeCN affords a mixture of $[Cp^*MoH_2(dppe)MeCN)]^+$ and $[Cp^*MoH(dppe)(MeCN)_2]^{2+}$, even when using less than 1 equiv of acid.[81] Analogously, the acidolysis of $MoH_4(PMe_2Ph)_4$ and $OsH_6(PPr^i_3)_2$ in MeCN with excess HBF_4 affords $[MoH_2(PMe_2Ph)_3(MeCN)_3]^{2+}$ and $[OsH_4(PPr^i_3)_2(MeCN)_2]^{2+}$, respectively.[60,113] In turn, the absence of the dicationic products cannot be taken as evidence ruling out a disproportionation mechanism, because path b.2 may be too slow relative to path b.1 to significantly contribute to the generation of products.

The decomposition mechanism of $[CpReH_2(PAr_3)_2]^+$ (Ar = *p*-C_6H_4X; X = H, Me, F, OMe) has been studied in detail, but this occurs only upon intervention of an electron-transfer-catalyzed pathway upon further oxidation.[63] There have been a number of other reports dealing with the decomposition of oxidation products of polyhydride species, but no detailed mechanistic studies have been carried out, nor have specific mechanistic proposals been advanced.[59,60,64] Generally, these lead only to the monocationic series of products. An exception is complex $MoH_4(PMe_2Ph)_4$, whose reaction with $AgBF_4$ in MeCN leads to $[MoH_2(PMe_2Ph)_4(MeCN)_2]^{2+}$ as the only product, although it has been suggested that Ag^+ may act as a hydride abstracting agent rather than an oxidant in this reaction.[60]

Finally, the possibility that oxidation induces a direct reductive elimination of H_2 (path c) should also be considered. A classical/nonclassical equilibrium for a 17-electron polyhydride complex has been suggested for $[Cp^*RuH_3(PPh_3)]^+$ and $[OsH_6(PPr^i_3)_2]^+$,[76,113] but a deprotonation (and not a H_2 loss) has been shown or suggested as the initial step for their decomposition. On the other hand, oxidation of dialkyl complexes is proven to favor alkyl−alkyl reductive elimination.[114−116]

(e) Decomposition Mechanisms of $[Cp^*MoH_3(dppe)]^+$ in THF and CH_2Cl_2. The decomposition of complex $\mathbf{1}^+$ following the oxidation of **1** in THF or CH_2Cl_2 (eq 3) represents the first unambiguous demonstration of an oxidatively induced H_2 elimination from a polyhydride complex. The reverse process, namely the oxidative addition of H_2 to a stable paramagnetic complex, had been established for the 15-electron complexes MCl_2L_4 (M = Nb, Ta; L = PMe_3 or L_2 = dmpe).[7] It should also be mentioned that an H_2 elimination was proposed to occur from Cp_2NbH_2 (generated in situ by H atom abstraction from Cp_2NbH_3), to generate a poorly characterized 15-electron Cp_2Nb transient, which was observed only as a fleeting intermediate by EPR spectroscopy.[117]

Proposals for the intimate mechanism of this transformation can be extrapolated from the well-studied diamagnetic counterparts as shown in Scheme 4.[118] The EPR signal decay is faster for $\mathbf{1}^+$-d_3 relative to that for $\mathbf{1}^+$, yielding an *inverse* isotope effect of 0.50(3). This strongly suggests a ground-state classical structure for complex $\mathbf{1}^+$, namely $[Cp^*Mo(H)_3(dppe)]^+$. A similar inverse isotope effect (0.4 ± 0.2) has been reported for the H_2 elimination from the classical dihydride complex $[Ir(H)_2(PPh_3)_2(nbd)]^+$ (nbd = norbornadiene).[119] The elimination of H_2 from a dihydrogen complex, i.e., of type $[Cp^*MoH(H_2)$-

(113) Smith, K.-T.; Tilset, M.; Kuhlman, R.; Caulton, K. G. *J. Am. Chem. Soc.* **1995**, *117*, 9473−9480.

(114) Pedersen, A.; Tilset, M. *Organometallics* **1993**, *12*, 56−64.
(115) Pedersen, A.; Tilset, M. *Organometallics* **1994**, *13*, 4887−4894.
(116) Fooladi, E.; Tilset, M. *Inorg. Chem.* **1997**, *36*, 6021−6027.
(117) Elson, I. H.; Kochi, J. K. *J. Am. Chem. Soc.* **1975**, *97*, 1262−1264.
(118) Crabtree, R. H. *Angew. Chem., Int. Ed. Engl.* **1993**, *32*, 789−805 and references therein.

$(dppe)]^+$ (**XI**), should lead to a normal (i.e., ≥ 1) isotope effect.[120] A classical structure is shown by the X-ray analysis for the W analogue $\mathbf{2}^+$ and is backed up by the DFT calculations on the $[CpWH_3(H_2PCH_2CH_2PH_2)]^+$ model system. As extensively documented for diamagnetic polyhydride systems, reductive elimination of H_2 from a 5d metal should be thermodynamically disfavored relative to that from a 4d metal.[121] It can thus be imagined that **X** or **XI** is more easily accessible for Mo than for W, rationalizing the much greater stability of complex $\mathbf{2}^+$ relative to that of $\mathbf{1}^+$ toward decomposition.

Path a involves a direct, one-step solvent-induced reductive elimination. This mechanism would be consistent with both the inverse isotope effect and the solvent dependence. However, it is difficult to rationalize, on the basis of this mechanism, the mechanistic diversion in MeCN (vide infra). The other pathways involve the intervention of the nonclassical intermediate **XI** in a first step, which could either be rate-determining or a rapid preequilibrium followed by a rate-determining replacement of the dihydrogen ligand by a solvent molecule. In the second case, the observed isotope effect on the decomposition rate would correspond to the combination of an *equilibrium isotope effect* for the first step and a *kinetic isotope effect* for the rate-determining exchange step. Inverse isotope effects were similarly interpreted for the reductive elimination of RH (via a R−H σ complex) from $Cp^*Ir(PMe_3)(C_6H_{11})(H)$ and from $Cp_2W(CH_3)(H)$.[122,123] The rate of decomposition should be solvent independent either if the first step is rate-determining or if the substitution of the H_2 ligand by the solvent is dissociative (via intermediate **XII**, path b in Scheme 4), whereas a solvent dependence is expected for a rate-determining associative exchange, either of the interchange type (I_a) or via a well-defined 19-electron solvent adduct **XIII** (path c). The faster decomposition process in CH_2Cl_2 relative to that in THF (see Results) suggests a rate-determining associative exchange (path c). On the basis of the better donor capability of THF relative to that of CH_2Cl_2, one would expect the opposite order of relative reactivity (THF > CH_2Cl_2). However, since the CH_2Cl_2 solvate of **3** has a 19-electron configuration (see Results), we assume that the acceleration effect for the decomposition in CH_2Cl_2 is due to the intervention of the second Cl atom in an interchange associative mechanism, facilitating the expulsion of the H_2 ligand.

(f) Decomposition Mechanisms of $[Cp^*MoH_3(dppe)]^+$ in MeCN. The different nature of the final products obtained by oxidation of **1** in MeCN (eq 2), together with the observation that **3** is relatively stable in MeCN, unambiguously shows that the decomposition of $\mathbf{1}^+$ cannot take place by reductive elimination of H_2 in MeCN as it does in THF and CH_2Cl_2. We should, therefore, consider the other two more usual pathways of proton transfer and disproportionation (paths a and b in Scheme 3). The most reasonable hypothesis for this mechanistic diversion is a greater susceptibility of the solvent adduct **XIII** to be oxidized by unsolvated $\mathbf{1}^+$, which results from the greater donating power of the MeCN ligand. Therefore, it is more likely that **XIII** is an intermediate along the reaction coordinate rather than a transition state (e.g., **X**). This pattern is well established from the previous studies on paramagnetic monohydride complexes.[57,75,112] The deprotonation mechanism is not a viable one if the oxidation is carried out stoichiometrically and if complex $\mathbf{1}^+$ is stable in MeCN *on the time scale of the oxidation process*, leaving no residual **1** to deprotonate $\mathbf{1}^+$. Furthermore, the stronger donor MeCN will make the adduct **XIII** a *weaker* acid relative to the same molecule having S = THF or CH_2Cl_2. Thus, a hypothetical deprotonation of **XIII** should be slower for S = MeCN. Since the stability of **XIII** when S = THF or CH_2Cl_2 is sufficiently long to allow the complete oxidation of **1** and the decomposition of $\mathbf{1}^+$ by H_2 elimination, it is extremely unlikely that $\mathbf{1}^+$ tranfers a proton to **1** before the latter is completely oxidized in MeCN.

The chemical nature of the products obtained from the rapid and stoichiometric oxidation of **1** in MeCN, notably the stereochemistry of the monohydride product, gives important information. The deprotonation mechanism would require that $[Cp^*MoH(dppe)(MeCN)_2]^{2+}$ is obtained as a secondary product by protonation of $[Cp^*MoH_2(dppe)(MeCN)]^+$ (Scheme 3). The protonation of $[Cp^*MoH_2(dppe)(MeCN)]^+$ by $HBF_4{\cdot}OEt_2$, however, was shown[81] to yield a *kinetic mixture* of two different isomers of the dication, the thermodynamically less stable isomer being favored over the more stable one by a 3:1 margin. A rationalization of this result[81] was based on a competition of the two inequivalent hydrides in a pseudo-trigonal prismatic structure for the proton, as indicated in **XIV**.

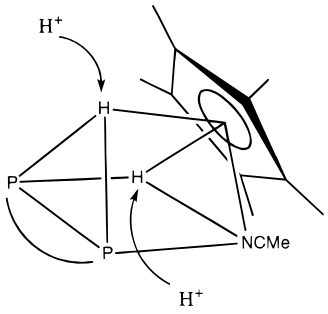

XIV

The observed stereochemistry could, in principle, be reconciled with the proton-transfer mechanism by invoking a 100% selectivity (discriminating ability) of the proton donor $\mathbf{1}^+$ toward one of the two inequivalent hydride positions, while the stronger acid $HBF_4{\cdot}OEt_2$ would not discriminate between the two inequivalent positions. It seems, however, more reasonable to assume that the decomposition follows the disproportionation pathway as proposed in Scheme 5. The formation of a single isomer of the monohydride dicationic product may then be easily rationalized by assuming that intermediate **XV** is stereochemically fluxional (dihydrogen/hydride complexes usually are), leading to a single most stable stereoisomer, and that the replacement of H_2 with a molecule of MeCN occurs stereoselectively. In case intermediate **XV** is stereochemically rigid, the observed result may still be rationalized if intermediate **XIII** is fluxional (17-electron complexes usually are), leading to a single isomer at this level.

A difference between the relative energies of the classical and nonclassical forms for the oxidized trihydride complexes $\mathbf{1}^+$ and $\mathbf{2}^+$ rationalizes well the different stability observed for the cations in MeCN. We propose that MeCN coordination can only take place for the nonclassical tautomer, which is only thermally accessible for the Mo system. Coordination to the classical tautomer to afford intermediate **XVI** is electronically

(119) Howarth, O. W.; McAteer, C. H.; Moore, P.; Morris, G. E. *J. Chem. Soc., Dalton Trans.* **1984**, 1171−1180.
(120) Hauger, B. E.; Gusev, D.; Caulton, K. G. *J. Am. Chem. Soc.* **1994**, *116*, 208−214 and references therein.
(121) Crabtree, R. H. In *Comprehensive Coordination Chemistry*; Wilkinson, G., Gillard, R. D., McCleverty, J. A., Eds.; Pergamon Press: Oxford, 1987; Vol. II, pp 689−714.
(122) Buchanan, J. M.; Stryker, J. M.; Bergman, R. G. *J. Am. Chem. Soc.* **1986**, *108*, 1537−1550.
(123) Bullock, R. M.; Headford, C. E. L.; Hennessey, K. M.; Kegley, S. E.; Norton, J. R. *J. Am. Chem. Soc.* **1989**, *111*, 3897−3908.

Scheme 5

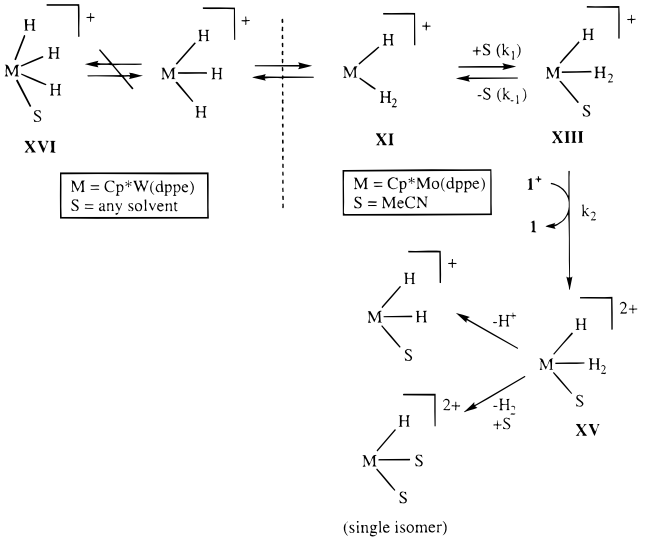

Scheme 6

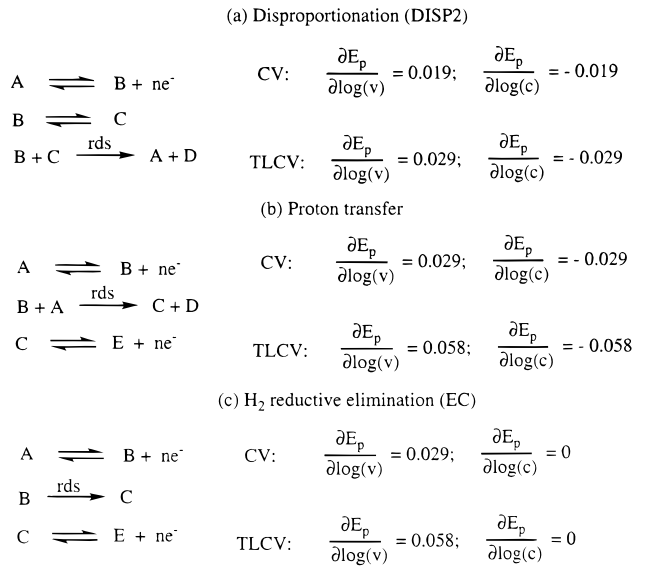

allowed but may experience a greater barrier because of a greater steric congestion. If coordination to the classical form were allowed, there would be no apparent reason for the much greater stability of $\mathbf{2}^+$ relative to that of $\mathbf{1}^+$ in MeCN because Mo and W have very similar atomic radii.

The proposition that disproportionation is the favored mechanism for the decomposition of $\mathbf{1}^+$ in MeCN is confirmed by the CV and TLCV studies (see Results). Because of the fast decomposition rate in MeCN, classical kinetic studies could not be carried out by EPR spectroscopy. On the other hand, the occurrence of the chemical decomposition process has a noticeable effect on the electron-transfer parameters, as measurable by a variety of voltammetric techniques, as already shown for other systems.[124]

For a CV experiment, according to the established theory, a mechanism involving a solvent-assisted disproportionation (Scheme 6a), whereby solvent coordination is rapid and the disproportionation step is rate determining (DISP2), [125] leads to a linear shift of the peak potential (E_p) relative to log(v) and log(c) in the kinetic zone (low scan rates), according to eq 7 (1 electron is involved in the electrochemical oxidation step).

$$E_p = E^\circ + 0.071 - 0.019 \log \frac{k_{disp} c}{v} \qquad \text{(CV)} \quad (7)$$

The peak potential, E_p, varies with a slope of 19 mV per log(v) unit and −19 mV per log(c) unit.[125] On the other hand, a mechanism involving a rate-determining proton transfer to the starting material (Scheme 6b) leads to a variation of E_p described by eq 8 (T = 20 °C).[126]

$$E_p = E^\circ + 0.058 - 0.029 \log \frac{k_{deprot} c}{v} \qquad \text{(CV)} \quad (8)$$

Shifts of E_p against log(v) and log(c) now have slopes of 29 and −29 mV, respectively, per log unit. Finally, a hypothetical H_2 reductive elimination mechanism (Scheme 6c), which is already established to take place in THF and CH_2Cl_2 *but not in MeCN*, yields a straight line for E_p vs log(v) with a slope of +29 mV per log unit, but the peak potential is independent of the concentration.[127] An alternative disproportionation mechanism which involves a rate-determining solvent coordination, followed by a rapid electron-transfer step (DISP1), would behave as a simple EC process (Scheme 6c).

The results are qualitatively the same *for the TLCV technique*, except that the slopes are now ±29 mV for the DISP2 mechanism (eq 9),[128] ±58 mV for the proton-transfer mechanism (eq 10)[129,130] and 58 mV (vs log(v)) and 0 (vs log(c)) for the EC mechanism.[129,131]

$$E_p = E^\circ + 0.055 - 0.029 \log \frac{k_{disp} c}{v} \qquad \text{(TLCV)} \quad (9)$$

$$E_p = E^\circ + 0.075 - 0.058 \log \frac{k_{deprot} c}{v} \qquad \text{(TLCV)} \quad (10)$$

The H_2 reductive elimination pathway can immediately be excluded for the decomposition in MeCN, since a concentration dependence is observed both in CV and in TLCV. Let us examine the experimental variation of the peak potentials vs log(v). In the kinetic region, the slope of the straight line is closer to 19 mV per log(v) unit in the CV (see Table 3), consistent with a DISP2 mechanism (eq 7). This is confirmed by the concentration dependence at constant scan rate (see Results). The TLCV data, however, yield a slope close to 58 mV in the E_{pa} vs log(v) plot (see Table 3), which is consistent with the proton-transfer mechanism rather than with the DISP2 mechanism.[132]

This apparently contrasting behavior can be rationalized by invoking the occurrence of both the disproportionation (DISP2) and the proton-transfer mechanisms in MeCN. Let us compare the results in CV with those in TLCV in the case of a DISP2 mechanism. The intercept, log(v_i), of the $E_{pa} = f(\log(v))$ curve

(124) Hammerich, O.; Parker, V. D. In *Organic Electrochemistry*; Lund, H., Baizer, M. M., Eds.; Marcel Dekker: New York, 1991; pp 121−206 and references therein.

(125) Mastragostino, M.; Nadjo, L.; Savéant, J. M. *Electrochim. Acta* **1968**, *13*, 721−749.

(126) Andrieux, C. P.; Nadjo, L.; Savéant, J. M. *J. Electroanal. Chem.* **1970**, *26*, 147−186.

(127) Nicholson, R. S.; Shain, J. *Anal. Chem.* **1964**, *36*, 706.

(128) Laviron, E. *J. Electroanal. Chem.* **1978**, *87*, 31−37.

(129) Laviron, E. *J. Electroanal. Chem.* **1972**, *39*, 1−23.

(130) Laviron, E. *J. Electroanal. Chem.* **1972**, *34*, 463−473.

(131) Laviron, E. *J. Electroanal. Chem.* **1972**, *35*, 333−342.

(132) We have taken into account only the points obtained for $v < 10^{-2}$ V s^{-1} for the determination of this slope. Above this value, the current has a diffusion component (the variation of i_p vs log(v) has a slope smaller than 1).

with the $E = E°$ axis leads to the chemical rate constant. When $E_{pa} = E°$, eqs 7 and 9 lead to the following:

$$\text{In CV} \qquad \log(k_{disp}c) = 3.55 + \log(\upsilon_{CV_i}) \tag{11}$$

$$\text{In TLCV} \qquad \log(k_{disp}c) = 1.90 + \log(\upsilon_{TLCV_i}) \tag{12}$$

The difference between eqs 11 and 12 leads to the relationship

$$\text{(DISP2 mechanism):} \quad \log(\upsilon_{TLCV_i}) = 1.65 + \log(\upsilon_{CV_i}) \tag{13}$$

Equation 13 shows that, for a pure DISP2 mechanism, the intercept in TLCV is shifted by 1.65 $\log(\upsilon)$ units with respect to that in CV. Analogous considerations for the pure deprotonation mechanism (eqs 14 and 15) show that the intercept in TLCV is shifted by 0.71 $\log(\upsilon)$ units with respect to that in CV (eq 16).

$$\text{In CV} \qquad \log(k_{deprot}c) = 2.00 + \log(\upsilon_{CV_i}) \tag{14}$$

$$\text{In TLCV} \qquad \log(k_{deprot}c) = 1.29 + \log(\upsilon_{TLCV_i}) \tag{15}$$

(proton-transfer mechanism):

$$\log(\upsilon_{TLCV_i}) = 0.71 + \log(\upsilon_{CVi}) \tag{16}$$

When the rate constants of the DISP2 reaction and the proton transfer are not too different, it is therefore possible to have a limitation by one mechanism in CV and by the other in TLCV. Experimentally, the DISP2 mechanism is rate-limiting in CV (slope of 19 mV) and the proton transfer is rate-limiting in TLCV (slope of 58 mV) (see Figure 3).

Experiments carried out at different concentrations give the intercepts indicated in Table 3. At each concentration, a value for $\log(k_{disp})$ may be calculated from the CV data and eq 11. Correspondingly, a value for $\log(k_{deprot})$ may be calculated for the TLCV data and eq 15. These values are also shown in Table 3. The results of the E vs $\log(\upsilon)$ and E vs $\log(c)$ experiments allow us to obtain average values of k_{disp} and k_{deprot} according to the following procedure. The representation of $\log(k\upsilon)$ as a function of $\log(\upsilon)$ must give a straight line of slope 1 and intercept equal to $\log(k)$. In the same fashion, the representation of $\log(kc)$ as a function of $\log(c)$ must give a straight line of slope 1 and intercept equal to $\log(k)$. We have therefore plotted the $\log(k\upsilon)$ and $\log(kc)$ data together against $\log(x)$ ($x = \upsilon$ or c, respectively) (see Figure 9). The linear fit of these data with an imposed slope of 1 gave $\log(k)$ as the intercept. The CV data (Figure 9a) yield a value of $\log(k_{disp}) = 3.60(1)$, or $k_{disp} = 3.98(9) \times 10^3\ s^{-1}\ M^{-1}$, whereas the TLCV data (Figure 9b) yield $\log(k_{deprot}) = 2.44(4)$, or $k_{deprot} = 2.8(2) \times 10^2\ s^{-1}\ M^{-1}$. The simulated voltammograms calculated with the DIGISIM 2.1 software,[78] for a mechanism where both DISP2 reaction ($k_{disp} = 4000$) and proton transfer ($k_{deprot} = 280$) are involved, lead to curves that fit well the experimental data, as shown in Figure 3 for one particular concentration.

The value of k_{disp}, according to Scheme 5, would be equal to $(k_1k_2/k_{-1})[S]$ and is therefore dependent on the nature of the solvent as previously discussed.[75] The ratio of the two second-order rate constants is $k_{disp}/k_{deprot} = 14(1)$. This ratio indicates that, when the concentrations of **1** and $\mathbf{1}^+$ (or rather, the sum of $\mathbf{1}^+$ and $\mathbf{1}(MeCN)^+$ in equilibrium) are equivalent, complex $\mathbf{1}^+$ is ca. 14 times more likely to remove an electron from $\mathbf{1}(MeCN)^+$ than to donate a proton to **1**. It is rare that both disproportionation and proton-transfer mechanisms may be observed at the same time for a 17-electron hydride complex. The only other previously reported case, to the best of our knowledge, is that of complex $[CpMoH(PMe_3)_3]^+$, for which $k_{disp}/k_{deprot} = 0.17(2)$ in THF.[112]

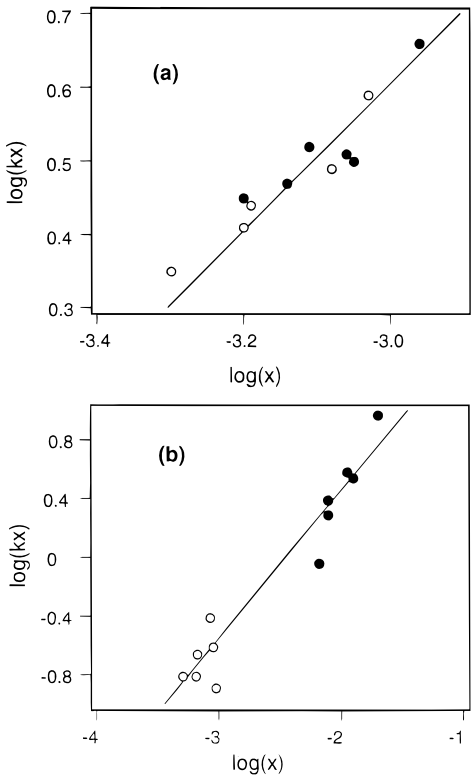

Figure 9. Plot of $\log(kx)$ vs $\log(x)$ (●, $x = \upsilon$ in V s^{-1}; ○, $x = c$ in mol L^{-1}) for (a) CV data and (b) TLCV data (see text).

The slow addition of a chemical oxidant (ferrocenium) to a MeCN solution of **1** supposedly simulates the conditions of the thin-layer electrochemical experiment. Thus, a greater proportion of $\mathbf{1}^+$ should decompose by the proton-transfer pathway, yielding more dihydride product. Indeed, this is experimentally observed (see Results). The monohydride product $[Cp^*MoH(dppe)(MeCN)_2]^{2+}$ is still obtained as a single isomer. This observation rules out a proton transfer to the dihydride product, $[Cp^*MoH_2(dppe)(MeCN)]^+$ (vide supra). It is logical to expect, however, that the protons released by $\mathbf{1}^+$ are captured by **1**, which is more basic and more abundant, to yield $[Cp^*MoH_2(dppe)(MeCN)]^+$, rather than by the latter to yield the monohydride complex. Thus, the monohydride complex derives *only* from the disproportionation pathway, whereas the dihydride product is at least partially produced by the deprotonation pathway under conditions of slow addition of the ferrocenium oxidant.

(g) Structure and Stability of Compound 3. The solution spectroscopic, conductivity, and electrochemical studies definitively prove that a solvent molecule is coordinated to **3** in solution, giving the ionic formulation $[Cp^*MoH(dppe)(S)]^+PF_6^-$. Thus, the complex belongs to the growing class of four-legged piano stool derivatives of Mo(III).[89] However, the solvent molecule must be very loosely coordinated because crystallization, even from MeCN, affords the solvent-free compound **3**, presumably containing a coordinated PF_6^-. The EPR spectroscopic properties of the CH_2Cl_2 adduct at low temperature (conditions in which the chemical exchange with free solvent is slow on the EPR time scale) show that the CH_2Cl_2 ligand adopts a chelating coordination mode, resulting in a formal 19-electron count for the complex. The facile coordination of donor solvents to 17-electron complexes in an equilibrium process with the 19-electron adduct has been frequently invoked to rationalize photochemical, electrochemical, and mechanistic observa-

tions[133,134] (including those discussed in this contribution, see section f above). The nature of the CH_2Cl_2 adduct of **3** provides a clear, direct demonstration of the accessibility of 19-electron complexes.

A final remark concerns the unexpected stability of **3** in all solvents, especially MeCN. As discussed in section d, cationic paramagnetic monohydride complexes are usually unstable, decomposing preferentially by either proton-tranfer or disproportionation mechanisms to afford more stable diamagnetic products. Since **3** is generated under conditions in which a base is not present, its decomposition by proton transfer cannot take place, but the disproportionation route is still viable. As we have argued in section f, even the disproportionation mechanism can be blocked when the size of the coordination sphere does not permit coordination of a solvent molecule and production of a more easily reduceable 19-electron adduct (rationalizing the stability of $\mathbf{2}^+$). Complex $[Cp^*MoH(dppe)(MeCN)]^+$, on the other hand, should be no more encumbered than complex $[Cp^*MoH(H_2)(dppe)]^+$, which disproportionates rapidly in MeCN. In addition, the likelihood of further MeCN coordination to $[Cp^*MoH(dppe)(MeCN)]^+$ is strongly suggested by the 19-electron configuration of $[Cp^*MoH(dppe)(\eta^2\text{-}Cl_2CH_2)]^+$. Decomposition of **3** in MeCN does eventually take place to afford $[Cp^*MoH(dppe)(MeCN)_2]^{2+}$ (the thermodynamically more stable isomer), $[Cp^*MoH_2(dppe)(MeCN)]^+$, and other yet uncharacterized products. This decomposition process will be the subject of further studies.

Conclusions

The studies reported in this contribution have raised a number of interesting issues.

The sterically encumbering Cp* and dppe ligands in complexes $\mathbf{1}^+$ and $\mathbf{2}^+$ reduce the kinetic acidity of the hydride ligands and disfavor the addition of donor solvents, stabilizing the complexes relative to the deprotonation and disproportionation pathways of decomposition, respectively. However, polyhydride complexes may decompose by yet another decomposition pathway, namely reductive elimination of H_2. The greater electron richness of W relative to that of Mo disfavors this decomposition for complex $\mathbf{2}^+$, which is therefore stable and can be isolated. Its X-ray structure shows that it is a classical trihydride complex. Conversely, complex $\mathbf{1}^+$ decomposes readily by what constitutes the first unambiguous example of oxidatively induced H_2 reductive elimination from a polyhydride complex.

The *inverse* isotope effect for the H_2 elimination from $\mathbf{1}^+$ suggests that this complex, like $\mathbf{2}^+$, adopts a classical structure. The solvent dependence on the rate of decomposition suggests a rate-determining associative mechanism for the replacement of H_2 by a solvent molecule.

In MeCN, the decomposition of complex $\mathbf{1}^+$ proceeds faster by a combination of disproportionation and (when the neutral precursor **1** is available) deprotonation. The relative rate of disproportionation and deprotonation [$k_{disp}/k_{deprot} = 14(1)$] has been measured by a combination of CV and TLCV studies. For the first time, a paramagnetic (poly)hydride system has been shown to decompose by one or more of three different mechanisms depending on conditions. Each of the three decomposition pathways has been quantitatively assessed.

The large difference in stability between the W (stable) and Mo (rapid decomposition) complexes in MeCN suggests that a solvent molecule easily coordinates to the Mo center in a thermally accessible, relatively open nonclassical structure of $\mathbf{1}^+$ but does not coordinate to the W center in the more crowded classical structure of $\mathbf{2}^+$.

Complex $\mathbf{2}^+$ adopts a novel and unusual geometry, which can be described as intermediate between octahedral and trigonal prismatic (when considering the Cp* as occupying a single coordination site) and is reproduced by DFT calculations on the $[CpWH_3(PH_2CH_2CH_2PH_2)]^+$ model system. This result represents circumstantial evidence in favor of an exchange mechanism which involves the interconversion of these two limiting structures, as also previously proposed for the neutral analogue.[81,93,96]

While a M−H bond weakening upon oxidation has previously been reported for other systems,[72,106,107] oxidation results in the strengthening of the metal−hydrogen bonds for both compounds **1** and **2** (and for the trideuteride analogues). This is experimentally shown by IR studies and is backed up by density functional calculations of bond lengths, BDEs, and M−H stretching frequencies. On the basis of first principles, we argue that compounds having a $M-H^{\delta-}$ bond polarity should always lead to M−H bond strengthening upon oxidation when the metal is electron-rich and the bond strength is dominated by the covalent component.

The product of H_2 elimination from $\mathbf{1}^+PF_6^-$, compound **3**, has a remarkable stability for a relatively unhindered paramagnetic hydride complex. This compound adds a solvent molecule when dissolved in MeCN, THF, or CH_2Cl_2. The latter is unambiguously shown by EPR spectroscopy to adopt a chelating coordination mode, yielding a 19-electron cation, $[Cp^*MoH(dppe)(\eta^2\text{-}Cl_2CH_2)]^+$. All these adducts, however, readily lose the solvent molecule in the solid state, giving back **3**.

Acknowledgment. We are grateful to the DOE (Grant DEFG059ER14230) and to the Région Bourgogne for support of this work. D.M. thanks the Région Bourgogne for a postdoctoral fellowship. We thank Mrs. Raveau-Fouquet for technical assistance.

Supporting Information Available: For the X-ray structures of compounds $[Cp^*WH_3(dppe)][PF_6]$ and $[Cp^*WH_4(dppe)][PF_6]$, tables of crystal data and refinement parameters, fractional atomic coordinates, bond distances and angles, anisotropic displacement parameters, and H-atom coordinates, and for the DFT calculations, tables of optimized geometric parameters for systems **III**−**IX** (PDF). Additional crystallographic data are available in CIF format. This material is available free of charge via the Internet at http://pubs.acs.org.

JA9834881

(133) Stiegman, A. E.; Tyler, D. R. *Comments Inorg. Chem.* **1986**, *5*, 215−245 and references therein.

(134) Tyler, D. R. *Acc. Chem. Res.* **1991**, *24*, 325−331 and references therein.